Characterizing Historical and Future Snowfall Events across the Western United States

BUREAU OF RECLAMATION

Final Report No. ST-2024-22071-01
Technical Report No. ENV-2025-024

Research and Development Office
Science and Technology
Research Program

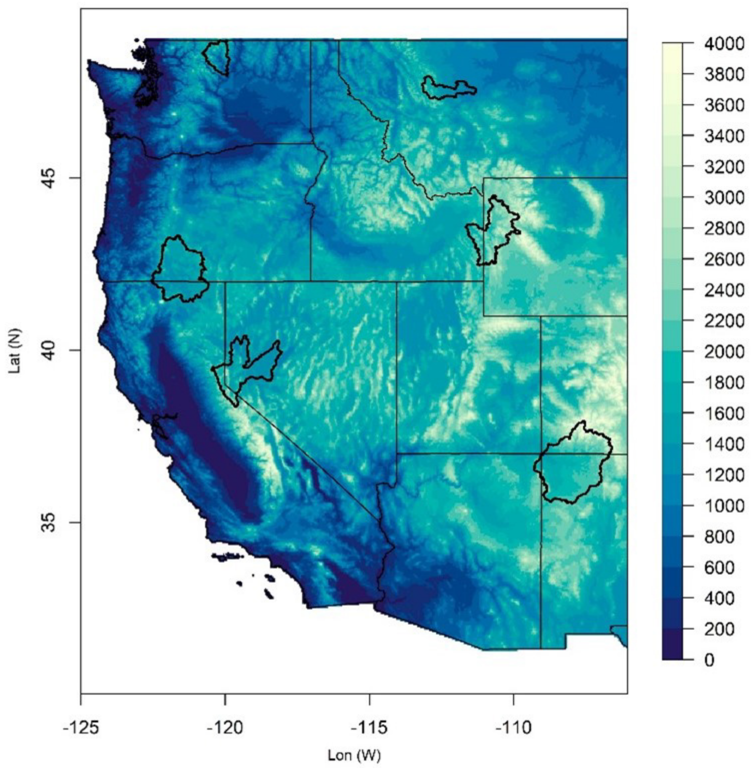

U.S. Department of the Interior

December 2024

REPORT DOCUMENTATION PAGE							*Form Approved* *OMB No. 0704-0188*

1. REPORT DATE (DD-MM-YYYY)	2. REPORT TYPE	3. DATES COVERED *(From - To)*
09/30/2024	Research	10/2022 – 12/2024

4. TITLE AND SUBTITLE
Characterizing Historical and Future Snowfall Events across the Western United States

5a. CONTRACT NUMBER
F597A

5b. GRANT NUMBER

5c. PROGRAM ELEMENT NUMBER
1541 (S&T)

6. AUTHOR(S)
Kathleen D. Holman, Ph.D.
Elise M. Madonna
David P. Keeney

5d. PROJECT ID NUMBER
Final Report No. ST-2024-22071-01

5e. TASK NUMBER

5f. WORK UNIT NUMBER

7. PERFORMING ORGANIZATION NAME(S) AND ADDRESS(ES)
Technical Service Center
Bureau of Reclamation
Denver, CO 80225

8. PERFORMING ORGANIZATION REPORT NUMBER
Final Report No. ST-2024-22071-01

9. SPONSORING/MONITORING AGENCY NAME(S) AND ADDRESS(ES)
Science and Technology Program
Research and Development Office
Bureau of Reclamation
U.S. Department of the Interior
Denver Federal Center
PO Box 25007, Denver, CO 80225-0007

10. SPONSOR/MONITOR'S ACRONYM(S)
Reclamation

11. SPONSOR/MONITOR'S REPORT NUMBER(S) (if applicable)
Final Report No. ST-2024-22071-01

12. DISTRIBUTION/AVAILABILITY STATEMENT
Final Report may be downloaded from https://www.usbr.gov/research/projects/index.html

13. SUPPLEMENTARY NOTES

14. ABSTRACT
In this study, we aim to improve understanding of heavy snowfall events across the Western United States by exploring the following three components of analysis. The first component includes describing historical snowfall events using point observations from the SNOTEL dataset in six Reclamation headwater basins. The second component involves characterizing weather types (e.g., atmospheric forcing) associated with the top eight heaviest historical snowfall events in each basin using the European Center for Mid-range Weather Forecasting's (ECMWF's) ERA-Interim reanalysis dataset (Dee et al. 2011) combined with the weather typing algorithm of Prein and Mearns (2021). The final component entails exploring simulation of historical weather types in climate projections from the Community Earth System Model version 2 (CESM2, Rodgers et al. 2021) Large Ensemble 2 dataset (LENS2). We focus on six Reclamation watersheds located in headwater regions, which include the Methow basin, WA, the Sun River basin, MT, the Upper Snake River basin, ID/WY, the Upper Klamath Lake basin, OR/CA, the Truckee-Carson basins, CA/NV, and the Upper San Juan basin, UT/AZ/CO/NM.

15. SUBJECT TERMS
Snowfall, weather typing, machine learning, clustering

16. SECURITY CLASSIFICATION OF:			17. LIMITATION OF ABSTRACT	18. NUMBER OF PAGES	19a. NAME OF RESPONSIBLE PERSON
					Kathleen Holman
a. REPORT	b. ABSTRACT	c. THIS PAGE			19b. TELEPHONE NUMBER *(Include area code)*
U	U	U		72	(303) 445-5271

Standard Form 298 (Rev. 8/98)
Prescribed by ANSI Std. Z39.18

Mission Statements

The U.S. Department of the Interior protects and manages the Nation's natural resources and cultural heritage; provides scientific and other information about those resources; honors its trust responsibilities or special commitments to American Indians, Alaska Natives, Native Hawaiians, and affiliated Island Communities.

The mission of the Bureau of Reclamation is to manage, develop, and protect water and related resources in an environmentally and economically sound manner in the interest of the American public.

Disclaimer

Acknowledgements

The authors would like to express gratitude to Dr. Andreas Prein for generously sharing expertise, data, and code with the team. The authors would also like to acknowledge computing support from the Casper system (https://ncar.pub/casper) provided by the National Science Foundation National Center for Atmospheric Research (NCAR), sponsored by the National Science Foundation

Cover Image – Cover image shows topography across the Western United States at 4-kilometer spatial resolution and the location of six Reclamation basins of interest in this study (Bureau of Reclamation).

Characterizing Historical and Future Snowfall Events across the Western United States

Final Report No. ST-2024-22071-01

Prepared by:

Technical Service Center
Kathleen D. Holman, PhD, Meteorologist
Elise M. Madonna, Physical Scientist
David P. Keeney, Meteorologist

Peer Review

Bureau of Reclamation
Research and Development Office
Science and Technology
Research Program

Final Report No. ST-2024-22071-01

Characterizing Historical and Future Snowfall Events across the Western United States

KATHLEEN HOLMAN Digitally signed by KATHLEEN HOLMAN
Date: 2024.12.13 15:49:48 -07'00'

Prepared by: Kathleen D. Holman, Ph.D.
Meteorologist, Applied Hydrology II

ELISE MADONNA Digitally signed by ELISE MADONNA
Date: 2024.12.16 10:12:57 -07'00'

Prepared by: Elise M. Madonna
Physical Scientist, Geographic Applications and Analysis

DAVID KEENEY Digitally signed by DAVID KEENEY
Date: 2024.12.16 09:58:32 -07'00'

Prepared by: David P. Keeney
Meteorologist, Applied Hydrology I

LINDSAY BEARUP Digitally signed by LINDSAY BEARUP
Date: 2025.01.21 08:32:40 -07'00'

Peer Reviewer: Lindsay Bearup, PE, Ph.D.
Civil Engineer (Hydrologic). Applied Hydrology I

This document has been reviewed under the Research and Development Office Discretionary peer review process, consistent with Reclamation Policy CMP P14. It does not represent and should not be construed to represent the Bureau of Reclamation's determination, concurrence, or policy.

Acronyms and Abbreviations

APR	Average Precision Recall
AR	atmospheric river
AUC	Area Under Curve
CESM2	Community Earth System Model version 2
CONUS	continental United States
CMIP6	Coupled Model Intercomparison Project Phase 6
DOI	U.S. Department of the Interior
ECMWF	European Center for Mid-range Weather Forecasting
ERA-Interim	ECMWF Reanalysis-Interim dataset
ESM	Earth System Model
ft	foot/feet
hPa	hectopascal
kg	kilogram
km	kilometers
LENS1	CESM1 Large Ensemble
LENS2	Large Ensemble 2
m^2	square meters
mm	millimeters
m/s	meters per second
N/A	not available; not applicable
Pa	Pascal
PRISM	Precipitation-elevation Regression on Independent Slope Model
Reclamation	Bureau of Reclamation
S&T	Science and Technology
SWE	Snow Water Equivalent
SNOTEL	SNOw TELemetry
TSC	Technical Service Center
UA SWE	University of Arizona's Snow Water Equivalent
U.S.	United States

WY	water year
XMT	extreme weather typing

Symbols

×	by
°	degree (latitude and longitude)
=	equal to
>	greater than
≥	greater than or equal to
<	less than
≤	less than or equal to
%	percent

Contents

Tables

Figures

Appendices

Executive Summary

Seasonal snowpack is a critical resource for water management across many parts of the world, including the Western United States (U.S.). Snow is often characterized by a variable called Snow Water Equivalent (SWE), which represents the depth of water obtained from melting a column of snow. Point and spatial estimates of SWE are used to inform local/regional water resource management, flood forecasting and hazards, climate studies, and wildfire risk assessments. While many researchers and practitioners recognize the importance of SWE, few studies focus on improving understanding of large snowfall events that drive snowpack growth.

In this study, we aim to improve understanding of snowfall events across the Western United States. by exploring the following three components of analysis. The first component includes describing historical snowfall events using point observations from the SNOw TELemetry (SNOTEL) dataset. The second component involves characterizing weather types (e.g., atmospheric forcings) associated with the top eight heaviest historical snowfall events in each basin of interest using the European Center for Mid-range Weather Forecasting's (ECMWF's) ERA-Interim reanalysis dataset (Dee et al. 2011). The final component entails exploring simulation of historical weather types in climate projections from the Community Earth System Model version 2 (CESM2, Rodgers et al. 2021) Large Ensemble 2 dataset (LENS2). We focus on six Bureau of Reclamation (Reclamation) watersheds located in headwater regions. The six basins include the Methow basin, WA, the Sun River basin, MT, the Upper Snake River basin, ID/WY, the Upper Klamath Lake basin, OR/CA, the Truckee-Carson basins, CA/NV, and the Upper San Juan basin, UT/AZ/CO/NM. Each of these basins is differentiated from the others by unique historical snowfall events and weather patterns.

In describing historical snowfall events in each basin, we quantify the number of days per water year with positive snowfall totals, maximum daily snowfall total per water year, and water year total snowfall among a subset of SNOTEL stations. Results suggest that the number of snowfall days is greatest in the Methow and Upper Klamath Lake basins, although annual water year total snowfall is often greatest in the Methow and Truckee-Carson basins. Water year maximum daily snowfall varies by SNOTEL station, where some of the largest daily totals are found at stations in the Upper San Juan and Truckee-Carson basins.

We investigate weather types associated with the eight heaviest historical snowfall events in each basin using the weather typing algorithm of Prein and Mearns (2021), where the number of weather types (e.g., clusters) varies by basin. Results show that two dominant weather types explain the historical heavy snowfall events in the Methow, Truckee-Carson, and Upper San Juan basins. Conversely, three weather types best describe forcing of the historical heavy snowfall events in the Snake, Sun, and Upper Klamath Lake basins. The dominant forcing mechanism of each historical weather type is summarized in table ES-1 with general descriptions of these terms provided in the body of the report.

Table ES-1.—Description of weather types responsible for the top eight largest snowfall events in each basin identified using observations from SNOTEL stations.

Basin/Weather Type	1	2	3
Methow basin	AR*-like	AR-like	NA
Snake River basin	AR-like	Upper-level trough	Cold front
Sun River basin	Cold front	AR-like	Upslope
Truckee-Carson basins	AR-like	AR-like	NA
Upper Klamath Lake basin	AR-like	AR-like	Cold front
Upper San Juan basin	Upper-level trough	Upper-level trough	NA

* AR: atmospheric river

Finally, we document how average atmospheric conditions from ten CESM2 LENS2 ensemble members compare with atmospheric conditions from the European Centre for Medium-Range Weather Forecasts Reanalysis-Interim dataset (ERA-Interim). We focus on atmospheric variables that are important to identifying historical weather types in each basin. We also map historical and future cool-season days from the ensemble members to historical weather types to explore seasonality. Collectively, these analyses support the characterization of historical heavy snowfall events across six Reclamation basins located in headwater regions using reanalysis and model simulations. Future work may explore changes in weather type, weather type frequency, and precipitation during those events.

Introduction

Background

Across the Bureau of Reclamation's (Reclamation) management domain, interannual variability in water resources can be large, and freshwater demands often exceed supply (Lute and Abatzoglou 2014). Cool season precipitation and high elevation snowpack are the foundation of water resources across this complex and diverse region of the United States (U.S.; Kapnick and Hall 2012). Snowpack provides natural storage of freshwater resources until the onset of snowmelt, when fresh melt water flows across the surface and into channels, eventually making its way to reservoirs (Hale et al. 2023). Many of the reservoirs located across the Western United States were built exclusively to store spring snowmelt and redistribute the freshwater resource to users at a later time (Kapnick and Hall 2010). Water managers are constantly balancing the need to store as much water as possible while also providing sufficient water for power generation, agricultural needs, recreation, and endangered species requirements (Serreze et al. 2001).

Western snowpack is typically observed by measuring snow water equivalent (SWE), a variable defined as the water content (in units of depth) of snow on the ground. SWE provides an integrated measure of snow accumulation and ablation processes (Lute and Abatzoglou 2014). Point observations and spatial estimates of SWE are used to inform streamflow forecasts at various time horizons and operational decisions (Reclamation 2021a). While the number of studies focusing on SWE across the Western United States is quite large, the number of studies investigating snowfall events is much smaller. The seasonal evolution of SWE is largely driven by snowfall events (McGinnis 1997; Serreze et al. 2001; Lute and Abatzoglou 2014), which can be identified by quantifying the daily change in SWE at a given location. Example time series of daily SWE and daily change in SWE for one site during a single water year (WY) are shown in figure 1.

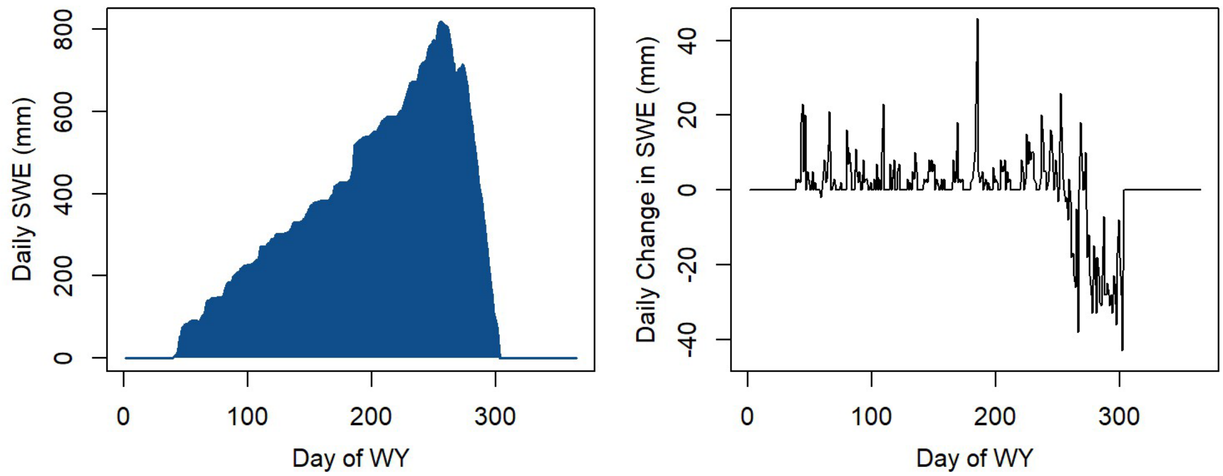

Figure 1.—(top) Sample time series of daily SWE (mm) at a single SNOTEL station for each day of water year (WY) 1991. (bottom) Sample time series of daily change in SWE (mm) at the same station for the same water year.

Serreze et al. (2001) explore the role and timing of large snowfall events contributing to high and low annual snowfall totals using observations recorded at 625 SNOTEL stations located across the Western United States, which they break down into eight distinct regions, between water years 1980 and 1998. Their results show that annual snowfall totals are greatest in the Sierra Nevada and Pacific northwest. Snowfall events across all regions can last more than one day, though 75 percent (%) of events in the Pacific Northwest and 89% of events in Arizona/New Mexico last 3 days or less. Their results also show that the leading snowfall event in each of the eight regions contributes anywhere from 10% in the Colorado region to 23% in Arizona/New Mexico to annual snowfall totals. This finding emphasizes the spatial heterogeneity in the contributions of single large snowfall events to annual totals. The timing of leading large snowfall events also varies by region. Large leading snowfall events in the Pacific Northwest tend to occur in the early winter (e.g., December and January), whereas large leading snowfall events in Utah tend to occur later in February and March (see figure 6 of Serreze et al. 2001 for more details).

Beyond characterizing heavy snowfall events, McGinnis (2000) examines the specific role of synoptic scale atmospheric circulation patterns in influencing snowfall in the Upper Colorado basin. His findings suggest that large snowfall events on the Colorado Plateau are associated with a trough of low pressure located off the southern California coast, which advects moist air into the region. More specifically, McGinnis (2000) states that this "low-pressure system is followed by a low-pressure system coming from the northern Pacific Gulf of Alaska that carries with it mechanisms for vertical motion and lower air temperatures. When this system reaches the Colorado River basin, the relatively moist air mass (combined with additional moisture advected from the Gulf of Mexico) is lifted and snowfall occurs." McGinnis (2000) clearly demonstrates a relationship between synoptic-scale atmospheric events and snowfall in the Upper Colorado basin.

Snowfall events in the Sierra Nevada have been linked to atmospheric rivers (ARs). ARs are synoptic-scale features of the atmosphere characterized by intense moisture transport concentrated in lowest 3 kilometers (km) of the atmosphere, with lengths that extend thousands of kilometers and widths that are an order of magnitude less (Payne et al. 2020). These systems incorporate moisture from local convergence and evaporation along their track, as well as from remote source regions in the tropics or subtropics (Payne et al. 2020). ARs can lead to catastrophic flooding when vast amounts of moisture impinge on topographic features across the Western United States (Corringham et al. 2019; Prince et al. 2021).

Guan et al. (2010) examine snowfall totals (i.e., positive changes in SWE) in the Snow Data Assimilation System (SNODAS) product (Carroll et al. 2001) during 45 wintertime ARs that struck the Sierra Nevada between 2004 and 2010. Their results suggest that AR events contributed between 30 and 40% of total seasonal SWE accumulation during the study years. Similarly, Demaria et al. (2017) examine the relationship between ARs, precipitation, and SWE during the cold season (defined as October through March) in the Salt and Verde basins of northeastern Arizona. Their results show that ARs can contribute upwards of 60% of total cool-season precipitation in the Salt and Verde River basins. Their results show that ARs are associated with mostly positive changes in basin-average SWE (see their figure 6 and figure 9).

Interest in linking snowfall events to atmospheric drivers is also growing outside the western United States Berger et al. (1999; 2003) identify four large-scale flow regimes that are responsible for snowfall events in the western Missouri region. Those four flow regimes are broadly categorized as progressive trough, southwest low, northwest low, and deepening low. Progressive troughs contribute the largest fraction to annual snowfall totals. Perry et al. (2007) classify all snowfall events in the Great Smoky Mountains National Park between 1991 and 2004 using a manual synoptic classification scheme. The authors generate composite maps of atmospheric conditions using the NCEP/NCAR reanalysis dataset. Their results suggest that more than 50% of mean annual snowfall occurs as a result of Miller A cyclones (Miller 1948) and low-level northwest flow.

Objectives

While progress has been made in classifying weather conditions conducive to heavy snowfall events in the central and eastern United States, there is a noticeable gap in understanding weather conditions related to heavy snowfall events across the Western United States. The current study aims to explore weather types associated with heavy snowfall events in a subset of Reclamation watersheds. The objectives of the current project are to (1) characterize historical snowfall events across the Western United States, (2) document weather types associated with historical heavy snowfall events using reanalysis data, and (3) examine how weather types conducive to observed heavy snowfall events are simulated in a large ensemble dataset. Global climate models struggle to simulate precipitation across scales and seasons (Nguyen et al. 2021 and references therein). Exploring weather types simulated by a large ensemble allows us to examine large scale weather conditions conducive to snowfall, rather than examining simulated snowfall itself. Further, the use of a large ensemble allows assessment of climate change in the presence of internal climate variability (Kay et al. 2015).

Study Watersheds

We focus the current investigation on six watersheds located in headwater regions across the Western United States (figure 2). From north to south, west to east, the basins of interest include: Methow basin, WA, Sun River basin, MT, Upper Snake River basin (also referred to as Snake Headwaters), ID/WY, Upper Klamath Lake basin, OR/CA, Truckee-Carson basins, CA/NV, and the Upper San Juan basin, UT/AZ/CO/NM. Topography across these basins is also shown in figure 2.

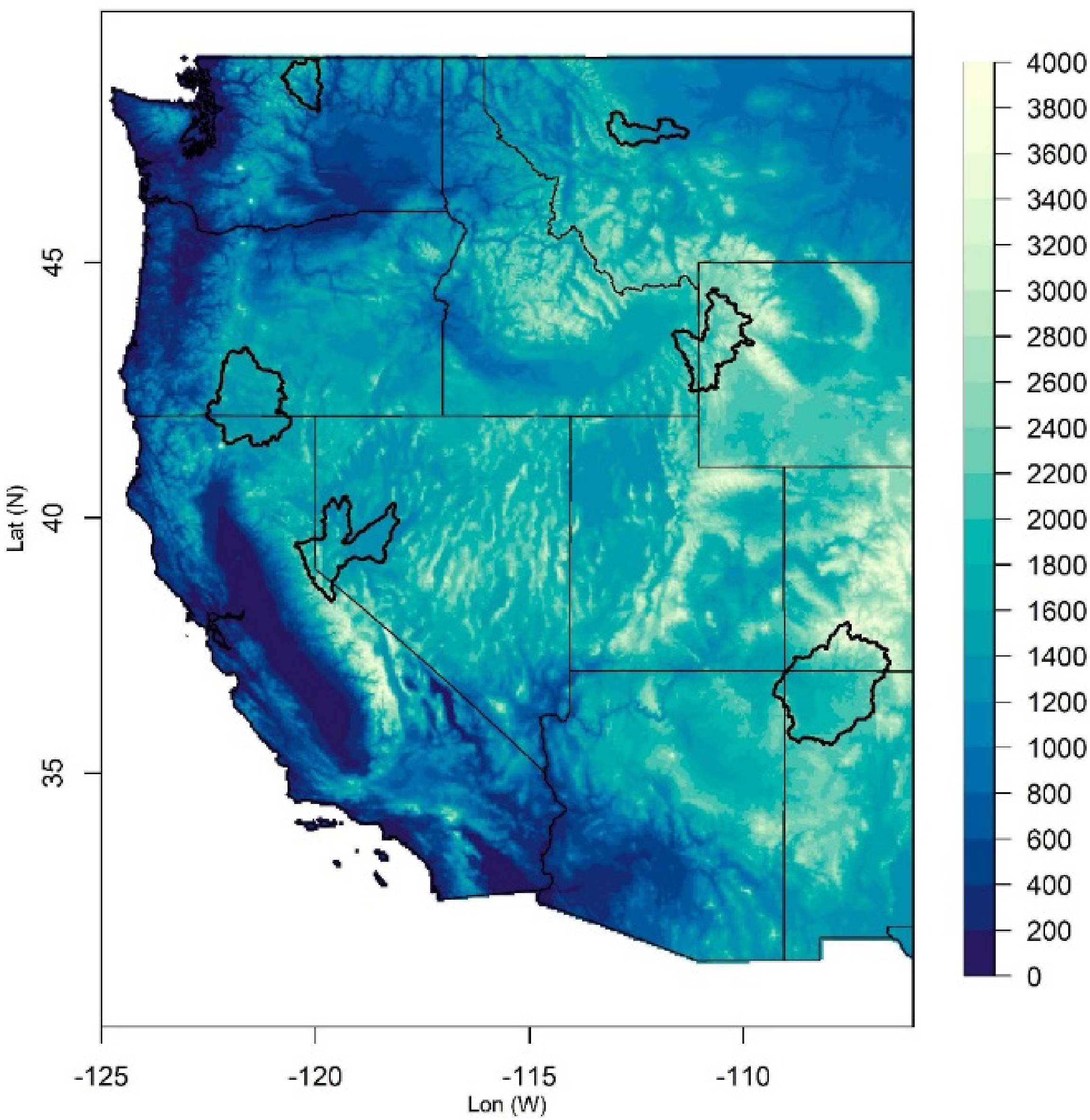

Figure 2.—Surface topography (m) at 4 km resolution across the Western United States from PRISM (Daly et al. 1994). Thick black lines represent watersheds of interest in this study: Methow, Sun, Upper Snake, Upper Klamath Lake, Truckee-Carson, and Upper San Juan.

Data

To meet study objectives, we employ a combination of data types and datasets, which include point observations, gridded precipitation and SWE products, historical reanalysis data, and model simulations. Point observations of SWE and snowfall equivalent serve as the basis of the analysis of historical heavy snowfall events. The gridded precipitation and SWE products provide spatial estimates of the two variables (precipitation and snowfall, respectively) during heavy snowfall events identified with point observations. The atmospheric reanalysis dataset is used as input to the weather typing algorithm to understand atmospheric forcing mechanisms (e.g., weather types) during heavy historical snowfall events. Model simulations, both historical and future, are used to understand how a single large ensemble captures weather types associated with historical snowfall events. The following sections describe these data in more detail.

Point Observations

SNOw TELemetry (SNOTEL)

This study focuses on point snow observations from a single dataset, the SNOTEL dataset. The SNOTEL dataset includes data from point stations generally located in high elevation regions that receive plentiful amounts of winter snowfall and at a minimum report air temperature, precipitation, snow depth, and SWE using an automated network maintained by the Natural Resources Conservation Service (NRCS; Fleming et al. 2023). According to Serreze et al. (2001), "SWE measurements at SNOTEL stations are made using snow pillows filled with an antifreeze solution. As the snow accumulates, the weight of the snowpack forces the solution into a manometer column inside the instrument shelter. The increase/decrease in manometer height is equal to the increase/decrease in SWE. A pressure transducer monitors the pressure of the fluid column and converts the pressure to SWE (in inches)."

We obtain SWE observations from SNOTEL stations located within 5 km of each individual watershed (figure 3). We use a 5 km threshold to identify neighboring stations located within similar hydroclimate conditions. One hundred sites meet the location criteria, with table 1 listing the final number of stations used for each basin. We utilize observations from these stations to characterize historical snowfall events, including heavy snowfall events.

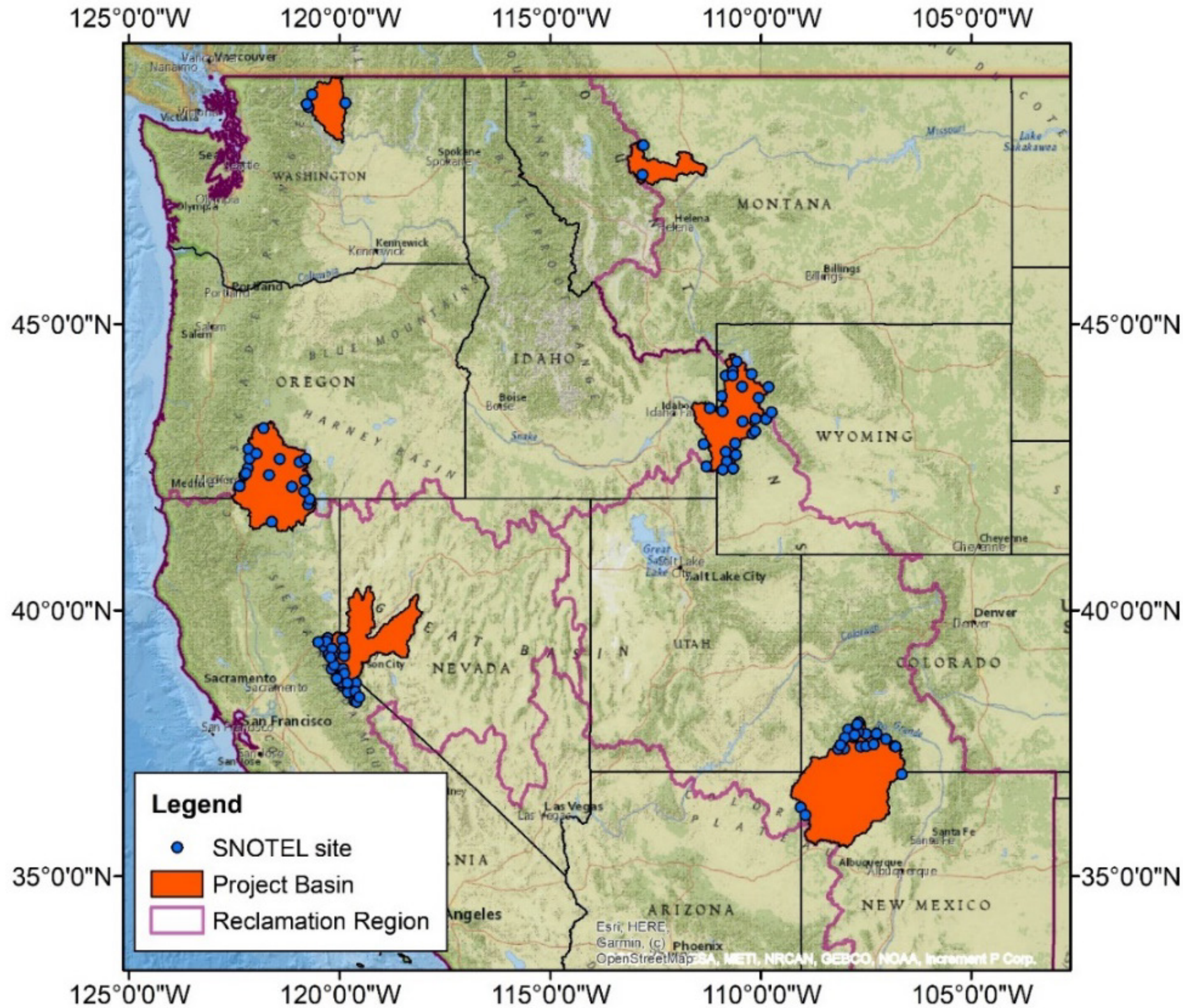

Figure 3.—Map showing SNOTEL stations located within 8 km of each basin and considered in the analysis.

Table 1.—Number of SNOTEL stations located within 8 km of each basin and with a non-zero number of historical observations.

Basin	Methow	Sun	Snake Headwaters	Upper Klamath Lake	Truckee-Carson	Upper San Juan
Number of SNOTEL stations	4	3	25	17	28	23

Gridded Precipitation Datasets

Precipitation-elevation Regression on Independent Slope Model (PRISM)

Oregon State University's PRISM Climate Group provides a 4 km gridded daily precipitation observation dataset for the contiguous United States (Daly et al. 1994). This dataset is created by using the Precipitation-elevation Regression on Independent Slope Model (PRISM) to fit the observed precipitation datapoints from about 20,000 stations onto a 4 km grid of precipitation estimates based on a climate-elevation regression and local properties that can affect climate (Daly, National Center for Atmospheric Research). A daily version of PRISM begins in 1981 and continues to the present day for all months of the year. However, to remain consistent with the gridded SWE and atmospheric reanalysis datasets (described below), we restrict data to the months of October through April between 1981 through 2018. This period of record is selected to align with a historical atmospheric reanalysis dataset used in weather typing, the European Centre for Medium-Range Weather Forecasts Reanalysis-Interim dataset (ERA-Interim; see description below). We utilize gridded precipitation estimates from PRISM to understand the spatial distribution of precipitation on observed heavy snowfall days identified using SNOTEL observations.

University of Arizona's Snow Water Equivalent (UA SWE)

The University of Arizona's Snow Water Equivalent (UA SWE) dataset provides daily 4 km SWE for the contiguous United States (Zeng et al. 2018; Broxton et al. 2019). SWE values in this dataset are created by combining SNOTEL and National Weather Service Cooperative Observer (COOP) station data with gridded fields from PRISM (Broxton and Zeng 2016). Measurements of SWE from the point sources are interpolated and normalized by net accumulated snowfall, estimated as accumulated snowfall minus accumulated snow ablation. Accumulated snowfall is determined by an air temperature threshold that can be adjusted to increase or decrease the amount of precipitation considered snow as opposed to rain, and ablation, which is a function of air temperature (Broxton and Zeng 2016). The interpolation method used to create this dataset allows SWE to be estimated using relatively few measurement stations (Broxton and Dawson 2016).

The full UA SWE dataset is available from WY 1982 (October 1, 1981) through WY 2022 (September 30, 2022). As with point observations, daily snowfall equivalent (SFE) is computed as the daily change in SWE. SWE values are converted to daily SFE by subtracting each day's total SWE from that of the previous day using the definition by Lute and Abatzaglou (2014). We exclude data from months between May and September (i.e., we include days from October through April). As with PRISM data, we include gridded SWE estimates from UA SWE as a means to understand the spatial distribution of snowfall on observed heavy snowfall days identified using SNOTEL observations.

Historical Reanalysis Data

Reanalysis datasets are used for a variety of hydrologic and atmospheric science applications, including seasonal hydrologic forecasting (Bastola and Misra 2014), SWE estimation (Casson et al. 2018), and annual water budgeting (Mahto and Mishra 2019), among others. In the current study, we use atmospheric fields (raw and computed) from ERA-Interim (Dee et al. 2011) to understand atmospheric conditions during historical heavy snowfall events in each of the six basins of interest. The European Centre for Medium-Range Weather Forecasts (ECMWF) has generated a global reanalysis dataset that includes hourly estimates of atmospheric climate variables from 1940 to present, referred to as ERA-Interim, as an update to ERA-40 (Uppala et al. 2005). The process of generating atmospheric fields in ERA-Interim includes a weather forecast model, a data assimilation method, and input datasets. The primary goals for ERA-Interim include updates to the hydrological cycle, enhancing the quality of stratospheric circulation, and improving the consistency in time of reanalyzed output fields. Raw and processed ERA-Interim fields are available between 1980 and present. However, processed and organized ERA-Interim files on the NCAR supercomputer end in 2018. Therefore, we analyze the period available in multiple datasets, which spans from October 1981 to December 2018. In the current study, variables from ERA-Interim (raw and processed) are used as inputs to the weather typing algorithm of Prein and Mearns (2021).

Climate Projections

The Community Earth System Model version 2 (CESM2) is one of the most comprehensive and complex Earth System Models (ESMs) available today (Simpson et al. 2020). The model contains interactive components for the atmosphere, land, ocean, sea ice, river transport, and land ice. The second Large Ensemble (LENS2) generated with CESM2 consists of 10 ensemble members at 1° latitude × 1° longitude spatial resolution covering the period 1850 to 2100 under SSP3-7.0 forcing protocols provided by the Coupled Model Intercomparison Project Phase 6 (CMIP6, Eyring et al. 2016). Unlike the first large ensemble, CESM1 Large Ensemble (LENS1), LENS2 uses a combination of oceanic and atmospheric initial states to create ensemble spread. The large ensemble design is experimentally similar to weather forecasts, in that one model is run many times with one set of boundary conditions and different initial conditions. This framework generates a distribution of outcomes consistent with the same assumptions (Mankin et al. 2020).

We utilize projections from CESM2 LENS2 to explore the simulation of identified weather types conducive to historical snowfall events in simulations. We utilize 10 ensemble members in the current investigation because daily fields have been saved for this subset of ensemble members. We utilize members from a large ensemble, as opposed to a collection of projections from different models, because the ensemble members represent a set of possible outcomes consistent with the same assumptions and forcings (Mankin et al. 2020).

Methods

We accomplish project objectives using datasets described above in conjunction with an array of technical methods. We characterize historical observed snowfall events by examining point records from SNOTEL stations available within and near the basins of interest. We compare spatial estimates of precipitation in two commonly applied gridded products, PRISM and UA SWE, on dates during heavy snowfall events identified using SNOTEL stations. We investigate the meteorological forcing of heavy snowfall events identified using SNOTEL observations in each basin using the weather typing algorithm of Prein and Mearns (2021). We document how average historical atmospheric conditions from ten CESM2 LENS2 ensemble members compare with atmospheric conditions in the ERA-Interim dataset. We focus on atmospheric variables that are important to identifying historical weather types in each basin. We map historical and future cool-season days from 10 CESM2 LENS2 ensemble members to each weather type identified for each basin. We use results from the mapping effort to understand if CESM2 LENS2 ensemble members simulate atmospheric conditions similar to historical conditions conducive to historical heavy snowfall events. The following sections describe these methods in more detail.

Weather Typing Algorithm

Overview

The extreme weather typing (XWT) algorithm used in this analysis is available in Prein and Mearns (2021) and summarized here. The XWT algorithm isolates the most extreme precipitation days from a historical dataset and sorts each day into a category, or weather type, according to the similarity in the atmospheric variable patterns between days. In this way, each extreme event from the gridded precipitation data is treated as a feature with associated atmospheric variables from ERA-Interim as attributes in the XWT algorithm's input data. The XWT algorithm works on a spatial domain that is defined by the region in a shapefile plus a 5-degree spatial buffer from all boundaries of the region. In this analysis, each basin is analyzed independently as its own region.

Prior to sorting the extreme days, the XWT algorithm preprocesses the data. First, the annual cycle and linear trends are removed to ensure that seasonal changes or long-term climate variability do not affect the weather typing (Prein and Mearns 2021). Next, relative anomalies are calculated for each extreme day based on mean climate conditions to minimize the effects of varying terrain, elevation, or other non-atmospheric, impacting factors across the area of study (Prein 2016). The final preprocessing step is to normalize the reanalysis fields to a mean of 0 and a standard deviation of 1 to ensure that the weather typing will not be skewed by combining input variables with different magnitudes (Milligan 1988).

The XWT algorithm utilizes hierarchical clustering followed by k-means clustering to group extreme precipitation days according to similarities and patterns in the reanalysis variables (Prein and Mearns, 2021). Pre-processed precipitation and reanalysis fields are input to the Ward's minimum variance hierarchical clustering algorithm. The hierarchical clustering algorithm generates clustering scenarios that range from including all data points in one large cluster to considering each data point as its own cluster. These scenarios are used in conjunction with the "elbow method" to determine the optimal number of weather types. The optimal number of weather types from Ward's minimum variance hierarchical clustering algorithm is then treated as an input to the k-means algorithm (Wilks, 2011). The elbow method works by considering the many cluster options generated by the hierarchical clustering algorithm and looking for the clustering step at which adding an additional cluster does not improve the percentage of variance in the data that is explained by the clusters (Bholowalia 2014). The number of clusters prior to this clustering step is then used as the number of clusters specified in the k-Means algorithm. This hybrid approach of two unsupervised machine learning models applied one after the other helps to overcome limitations associated with each model individually: neither the level of granularity in sorting for hierarchical clustering nor the initial seed selection for k-means need to be explicitly set by the user (Qi et al 2017). Schiemann and Frei (2010) suggest that this combination of methods categorizes weather patterns particularly well, preventing the need for set values by sequentially applying these two clustering algorithms results in an approach that is much more robust across varying datasets for different regions.

Atmospheric Variables

The number of possible atmospheric variables to include when running the weather typing algorithm is large. Optimization tools from Prein and Mearns (2021) test algorithm performance using combinations of up to four atmospheric variables. However, their results suggest that combinations of more than three variables do not add skill to the weather typing algorithm. We therefore test combinations of up to three atmospheric variables. A list of atmospheric variables considered in the historical analysis is shown in table 2. Moisture flux at a given pressure level is computed following Prein and Mearns (2021).

Table 2.—Atmospheric variables considered in the weather typing algorithm

Long Name	Short Name	Units
Sea level pressure	PSL	Pa
Specific humidity at 850 hPa	Q850	kg kg^{-1}
Specific humidity at 500 hPa	Q500	kg kg^{-1}
Air temperature at 850 hPa	T850	K
Air temperature at 500 hPa	T500	K
Geopotential height at 500 hPa	ZG500	m^2 s^{-2}
Meridional wind speed at 700 hPa	V700	m s^{-1}
Horizontal wind speed at 200 hPa	UV200	m s^{-1}
Moisture flux at 850 hPa	MFL850	(kg m) (kg s)$^{-1}$
Moisture flux at 500 hPa	MFL500	(kg m) (kg s)$^{-1}$

Pa=Pascal; hPa=hectopascal; K=Kelvin; Kg=kilogram;M^2=square meter; m=meter; s=second

Skill Scores

Skill scores are used as a metric to compare the XWT algorithm's performance over varying basins and precipitation datasets and to select the optimal reanalysis data predictors used to weather type the conditions for each individual basin. Two main skill scores are used for variable selection: Area Under Curve (AUC) and Average Precision Recall (APR). These metrics are used together in part because they are uncorrelated, and they are commonly used for model performance testing and validation (Rosset 2004; Cook 2020). In the context of this analysis, the AUC score is the probability of the model distinguishing correctly between two extreme precipitation days that belong to two different weather types. The APR score measures the model's precision as in distinguishing extreme precipitation days from non-extreme days based on the reanalysis data patterns and characteristics identified in each extreme weather type. When used for variable selection, these scores indicate the variable combination that best distinguishes extreme days from each other to allow the XWT algorithm to sort the days into distinctive weather types and then identify which weather type is most fitting for new extreme days. Optimal reanalysis fields are selected independently for each basin to fit the unique weather patterns and forcing mechanisms present in each basin.

In addition to variable selection, the AUC and APR skill scores are used to tune the model settings of number of extreme days and number of reanalysis data predictors used for clustering. Skill scores among weather types improve when fewer extreme days are included in the initial pool of events. This occurs due to the smaller number of days being mapped to each possible weather type. However, greater specificity in model fit results in less robustness for new data points that vary from the events used to train the model, or in this case, create the existing weather types. Therefore, the number of extreme days was chosen to encourage the creation of weather types specific and distinct enough to provide good fit for the days in them while also being general enough to represent more than one individual day. After testing between six and 40 extreme days, tests showed that eight extreme days, the top 0.1% of the input days, provided the most favorable results. Similar considerations were relevant when determining the optimal number of reanalysis fields to be used by the XWT algorithm. Increasing the number of variables provides more information which can be used to find similarities and differences in the extreme days; however, more variables also increase the amount of noise present within a cluster and can make it more difficult to identify meaningful patterns. The number of reanalysis variables used for sorting was varied from one to four. Following Prein and Mearns (2021), we ultimately ran the XWT algorithm with up to three atmospheric variables.

Beyond skill scores, we use Euclidean Distance (ED) and Manhattan Distance (MD) as quantitative performance metrics for mapping simulated days to weather types in each basin. ED calculates the shortest straight-line distance between two points in a multi-dimensional space. Mathematically, for two points, $P(x_1, y_1)$ and $Q(x_2, y_2)$, ED is computed as

$$ED = \sqrt{(x_2 - x_1)^2 + (y_2 - y_1)^2} \tag{1}$$

The Euclidean distance represents the shortest path between two points, akin to a straight line (Suwanda 2020). MD, also known as "taxicab" or "city block" distance, measures the total absolute differences across all dimensions (Suwanda 2020). For the same points, P and Q, MD is computed as

$$MD = |x_2 - x_1| + |y_2 - y_1| \quad (2)$$

MD reflects a path that follows grid lines, similar to navigating through city streets. For both ED and MD, lower values indicate better agreement (i.e., shorter distances between variables).

Future Analysis

After using the XWT algorithm to categorize each of the eight historical days into weather types and to calculate a centroid for each weather type, CESM2 LENS2 days from October through May for the historical period (1982 to 2018) and the future period (2062 to 2098) are compared to each possible weather type for each basin. Prior to mapping future days to historical weather types, the ensemble data were preprocessed and normalized using the same methodology applied to historical data. Next, to sort each ensemble date into a weather type, the Euclidean distance (ED) and Manhattan distance (MD) are calculated between each ensemble day and each weather type centroid (Aggarwal et al. 2001; Prein et al. 2023). We explore weather types using both ED and MD.

Glossary

Here, we list and summarize a subset of common atmospheric drivers of precipitation (including solid precipitation) that are relevant to weather typing results in this study. Definitions below come from multiple sources, including the American Meteorological Society's Glossary of Meteorology (available at https://glossary.ametsoc.org), the National Weather Service's Glossary (available at https://forecast.weather.gov/glossary.php), Wikipedia, and Google AI results.

Atmospheric river: A long, narrow, and transient corridor of strong horizontal water vapor transport that is typically associated with a low-level jet stream ahead of the cold front of an extratropical cyclone. The water vapor in atmospheric rivers is supplied by tropical and/or extratropical moisture sources. Atmospheric rivers frequently lead to heavy precipitation where they are forced upward, for example, by mountains or by ascent. Horizontal water vapor transport in the midlatitudes occurs primarily in atmospheric rivers and is focused in the lower troposphere. Atmospheric rivers are the largest "rivers" of fresh water on Earth, transporting on average more than double the flow of the Amazon River.

Low pressure system: In meteorology, an "area of low pressure," referring to a minimum of atmospheric pressure in two dimensions (closed isobars) on a constant-height chart or a minimum of height (closed contours) on a constant-pressure chart. Since a low on a synoptic chart is always associated with cyclonic circulation, the term is used interchangeably with cyclone.

Other names: depression

Cold front: Any nonoccluded front, or portion thereof, that moves so that the colder air replaces the warmer air; that is, the leading edge of a relatively cold air mass. A cold front is the leading edge of a cooler mass of air at ground level that replaces a warmer mass of air and lies within a pronounced surface trough of low pressure. It often forms behind an extratropical cyclone (to the west in the Northern Hemisphere, to the east in the Southern Hemisphere), at the leading edge of its cold air advection pattern—known as the cyclone's dry "conveyor belt" flow. Temperature differences across the boundary can exceed 30°C from one side to the other. When enough moisture is present, precipitation can occur along the boundary. If there is significant instability along the boundary, a narrow line of thunderstorms can form along the frontal zone. Cold fronts are stronger in the fall and spring transition seasons and are weakest during the summer.

Upslope flow (NWS): Air that flows toward higher terrain, and hence is forced to rise. Rising air cools and can result in precipitation. The added lift often results in widespread low cloudiness and stratiform precipitation if the air is stable, or an increased chance of thunderstorm development if the air is unstable.

Other names: orographic lifting

Upper-level trough: A low-pressure area that forms in the upper atmosphere, typically two to five miles above the Earth's surface. Upper-level troughs are created by atmospheric processes, such as:
air mass convergence, rising air, and atmospheric disturbances. The Earth's rotation and the presence of mountains can also influence trough formation. Upper-level troughs can lead to hazardous weather, including low cloud ceilings, precipitation with low visibility, icing, convective storms, and sudden wind shifts and strong wind gusts. The severity of these hazards depends on the characteristics of the trough and the surrounding air mass.

Other names: upper trough, upper-air trough, high-level trough, upper-level low

Results

Historical Snowfall Events

We characterize historical snowfall events in basins of interest to this study by examining snowfall events, which we define as days on which the change in SWE is positive and greater than a trace (a trace is defined as 0.1 in or 2.5 millimeters [mm]). Figure 4 shows the average number of days per month when snowfall occurred during each site's respective period of record (symbol color varies by SNOTEL station). The largest average number of snowfall days per month occurs in the Methow (17 days in November, December, and January) and Upper Klamath basins (18 days in March). The lowest average number of snowfall days per (winter) month occurs in the Truckee-Carson (3 days in October) and Sun River basins (4 days in October).

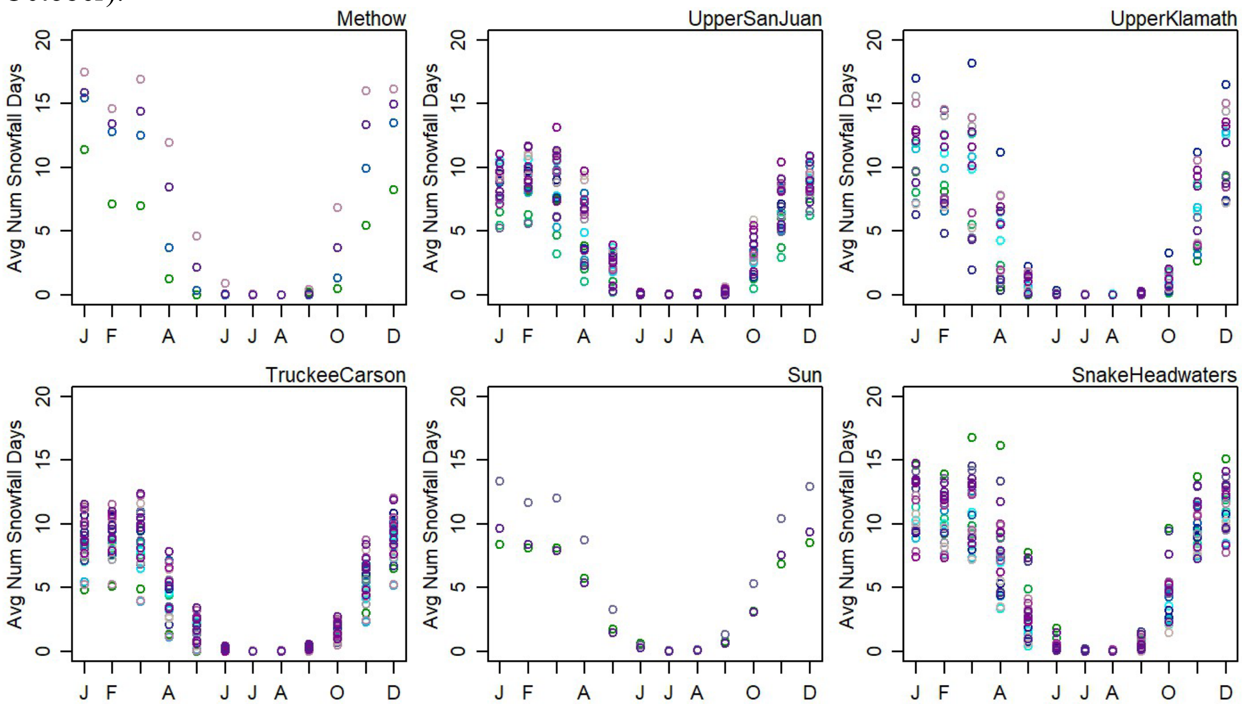

Figure 4.—Average number of snowfall days per month at each SNOTEL station. Color represents different SNOTEL stations.

Figure 5 shows the relationship between water year total snowfall (y-axis) and the number of snowfall days (in the same water year) for all years of data at each SNOTEL station. Similar results are shown in figure 6, except only the means are plotted (one point per SNOTEL station). Water year total snowfall values are greatest in the Truckee-Carson and Methow basins and are lowest in the Sun River basin.

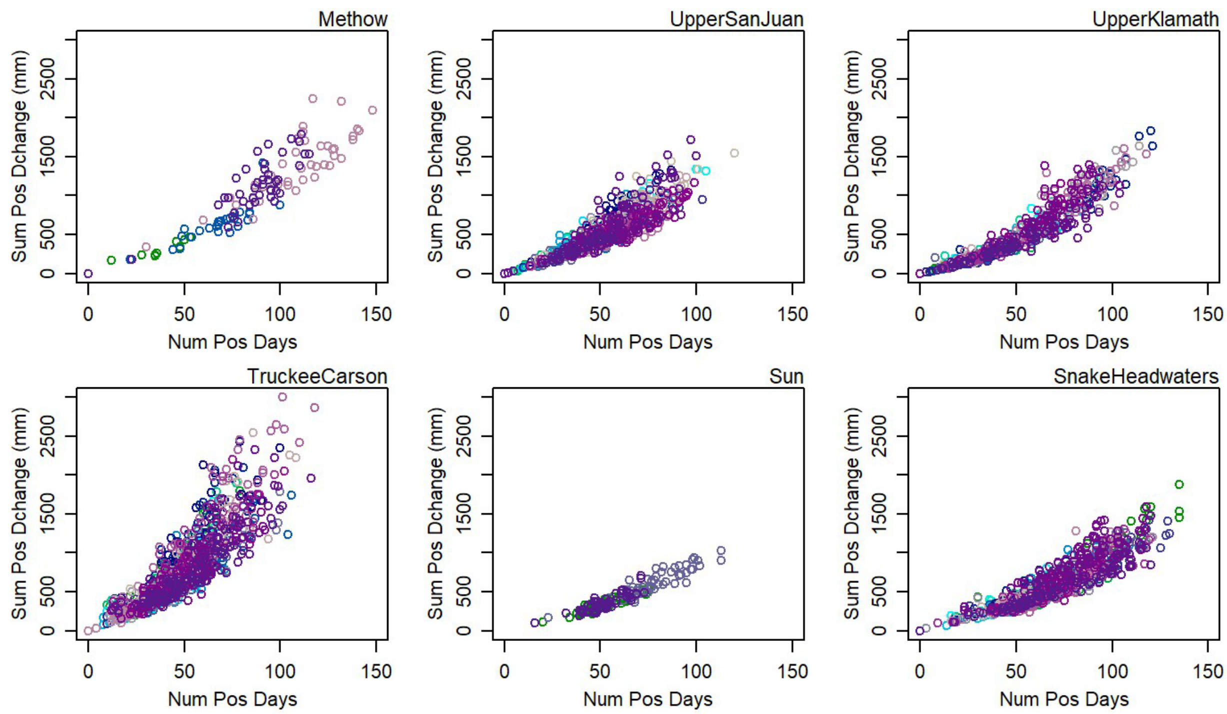

Figure 5.—Scatterplots showing the water year sum of snowfall (mm) versus the number of snowfall events per water year. Each circle represents a water year. Each color represents a SNOTEL station.

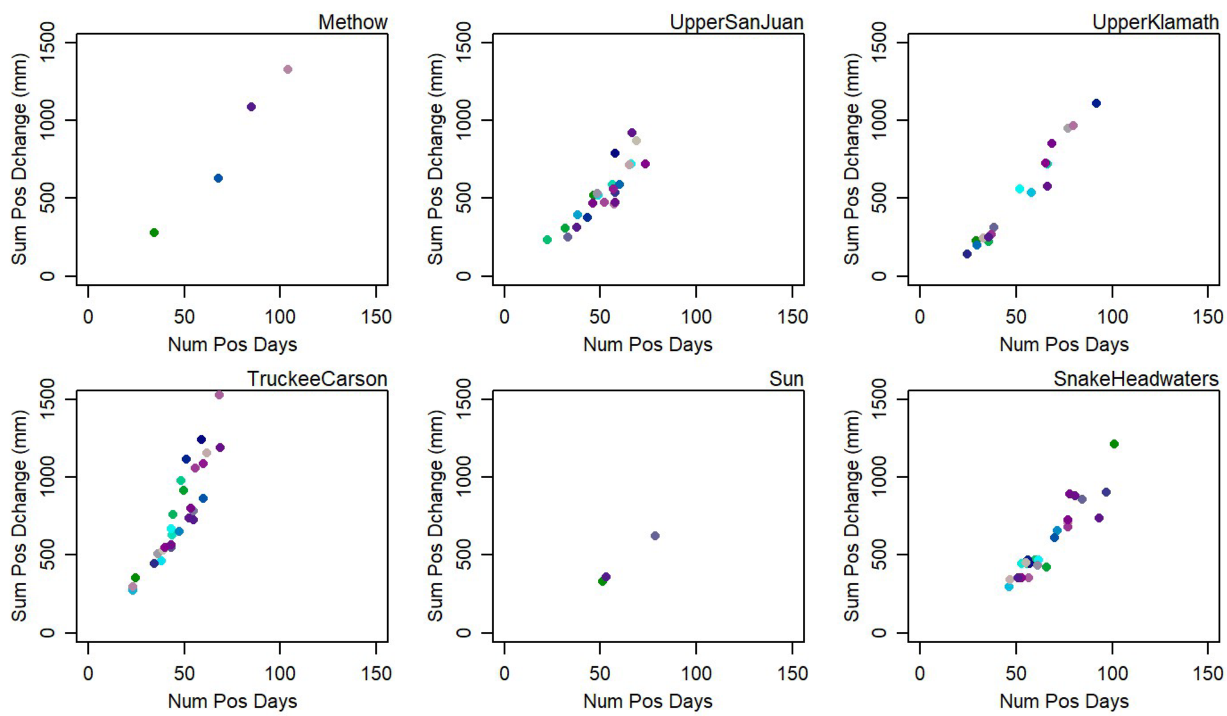

Figure 6.—Station-mean values of data presented in figure 5, such that there is one filled circle per SNOTEL station.

The distributions (via box and whisker plots) of water year maximum daily snowfall as a function of SNOTEL station are summarized in figure 7. Results show that the largest daily snowfall totals occur in the Truckee-Carson basin and the lowest water year maximum daily snowfall totals occur in the Sun River and Snake River basins. These box and whisker plots also demonstrate how water year maximum daily snowfall totals vary within each basin.

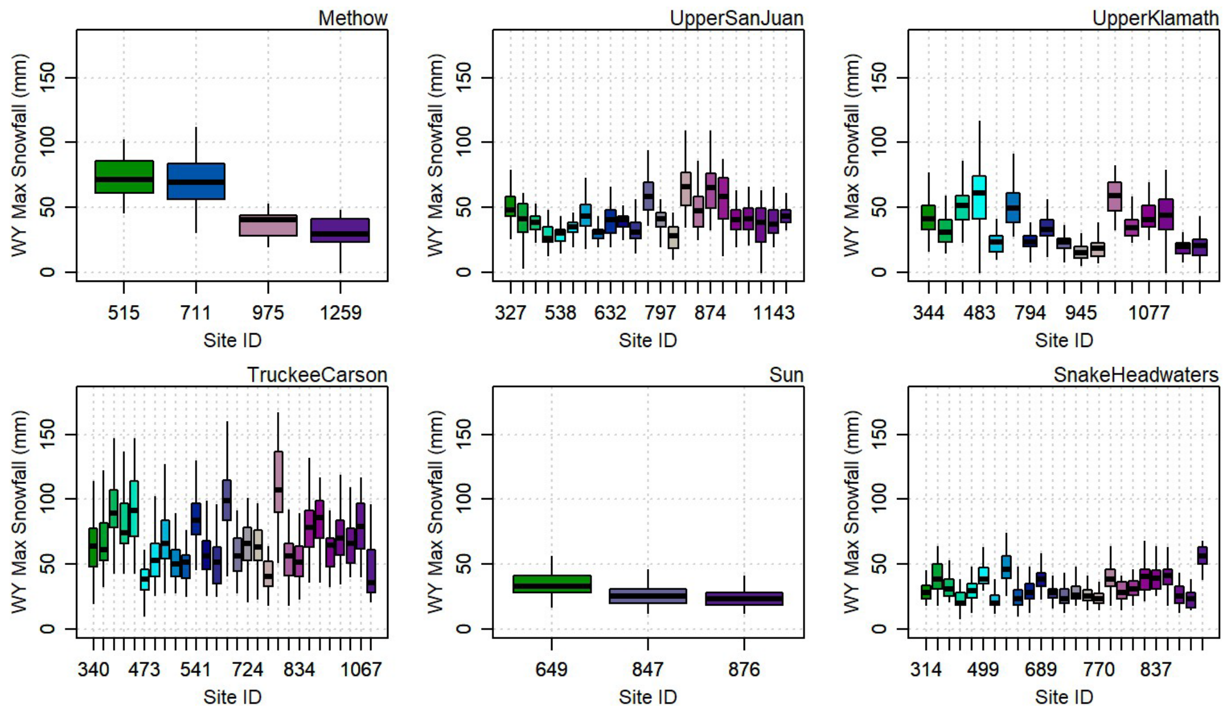

Figure 7.—Box and whisker plots of water year maximum snowfall (mm) at each SNOTEL station.

Results in figure 8 show box and whisker plots of fractional contribution of water year maximum snowfall to water year total snowfall for all possible years and stations. These plots show interesting behavior among stations and among basins. For example, in the Upper San Juan basin, one station shows a median fractional contribution to water year total snowfall of almost 15% while many other stations associated with the basin show median fractional contributions between 5% and 10%. As with the Upper San Juan basin, two SNOTEL stations associated with the Truckee-Carson basins show median fractional contributions near or at 15%. Median fractional contributions in the Methow, Sun, and Snake basins are largely between 5% and 10%. Median fraction contributions in the Upper Klamath basin range between 5% and 13%.

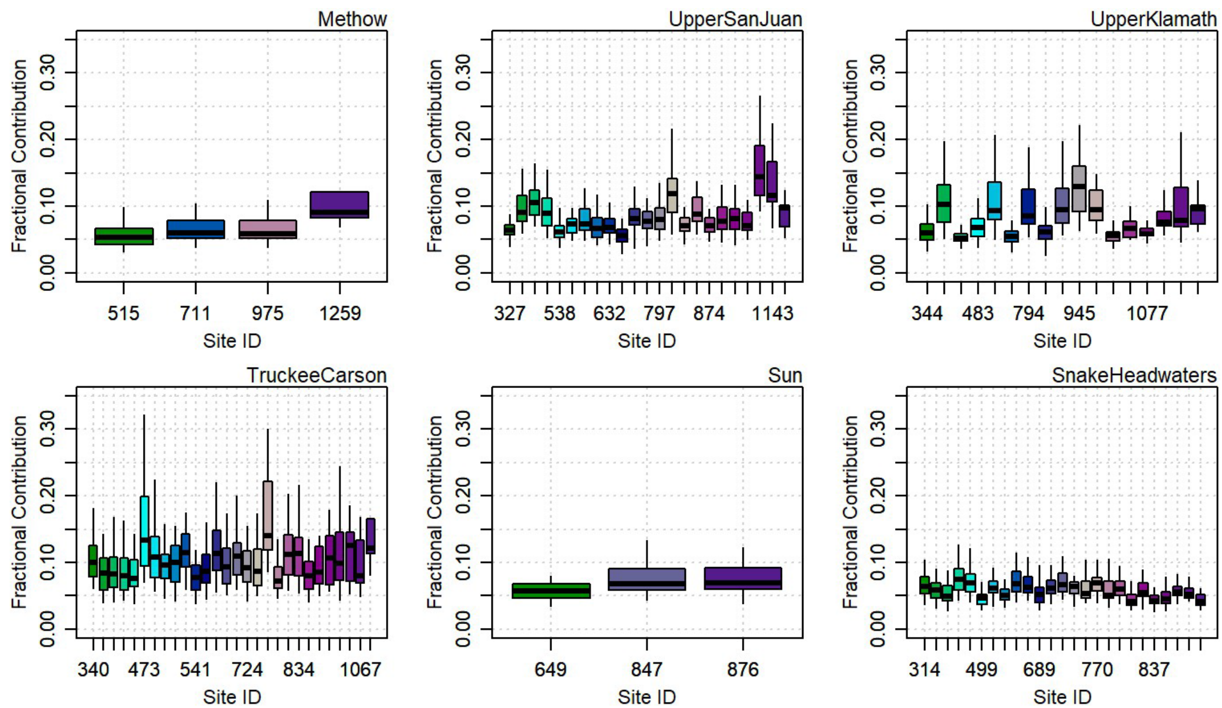

Figure 8.—Box and whisker plot of water year max daily snowfall to water year total snowfall (i.e., fractional contribution) for each SNOTEL station.

We compute daily snowfall equivalent at each SNOTEL station for a basin, average all snowfall totals together for each date in the historical record, and rank those average totals from largest to smallest. Although these analysis steps allow the number of stations to vary as a function of date (e.g., not all stations report on every day of the historical record), we do not filter out stations for record completeness to retain as many stations in the analysis as possible. Events that occur within seven days of an existing top event (on either side) are removed. Stated differently, we retain the greatest daily event among events that occur within seven-day windows of one another. The threshold is similar to the threshold employed by others to eliminate events caused by the same synoptic event (Prein and Mearns 2021). Results in figure 9 indicate that the largest single day average snowfall occurs in the Truckee-Carson basin, followed by the Methow basin, and is lowest for the Snake River basin. Among the basins, average daily snowfall totals among the top 8 events from the Truckee-Carson and Methow stations exceed those in the other four basins. Daily totals in the Sun River and Snake Headwater basins are remarkably similar beyond the first three events. Historical dates corresponding to the top 8 events in each basin are listed in appendix B.

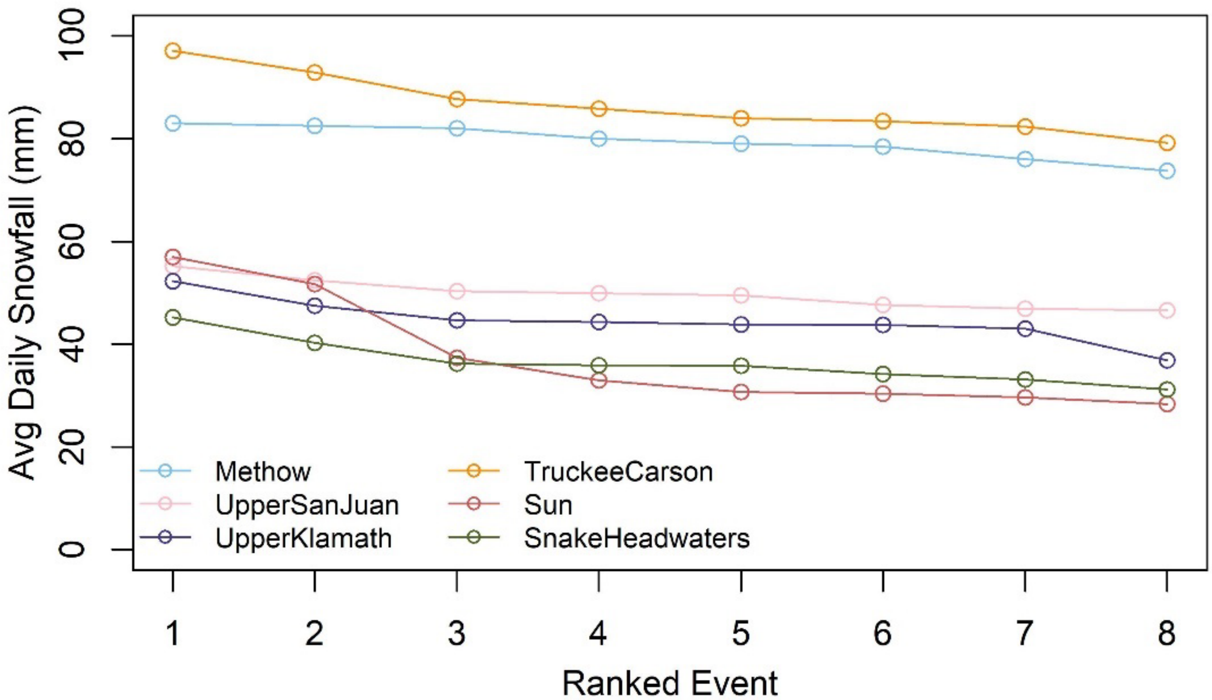

Figure 9.—Top eight average daily snowfall totals (mm) between January 1982 and December 2018 from all SNOTEL stations in each basin.

While observations from SNOTEL stations provide critical details on point snowfall totals, they do not provide information on how snowfall varies spatially across basins. To understand spatial distributions of precipitation during heavy snowfall events identified from SNOTEL stations, we extract UA SWE snowfall data and PRISM precipitation data on the top 8 heaviest SNOTEL events (dates extracted from events ranked in figure 9). We focus on these two gridded datasets because a) they are of high spatial resolution, which is important for precipitation in regions of complex topography; b) they are both used throughout the water resources community; and c) PRISM data inform UA SWE estimates. Temporal averages of UA SWE snowfall and PRISM precipitation grid cell by grid cell on the top 8 heaviest snowfall events identified in SNOTEL stations are shown in figure 10 and figure 11, respectively. Average snowfall totals from UA SWE largely follow topographic features of the land surface, with enhanced snowfall totals seen in regions of higher elevations. The largest snowfall totals among basins occur in the Methow and Truckee-Carson basins, in agreement with point SNOTEL observations. Spatial distributions of average precipitation (among the top 8 events) from PRISM resemble the spatial distributions of snowfall from UA SWE, albeit with lower magnitudes across nearly all basins. PRISM also shows greater average precipitation depths in the Methow and Truckee-Carson basins. Average PRISM precipitation depths are quite low in the Upper San Juan, Upper Klamath, and Sun River basins, even in regions with higher elevations.

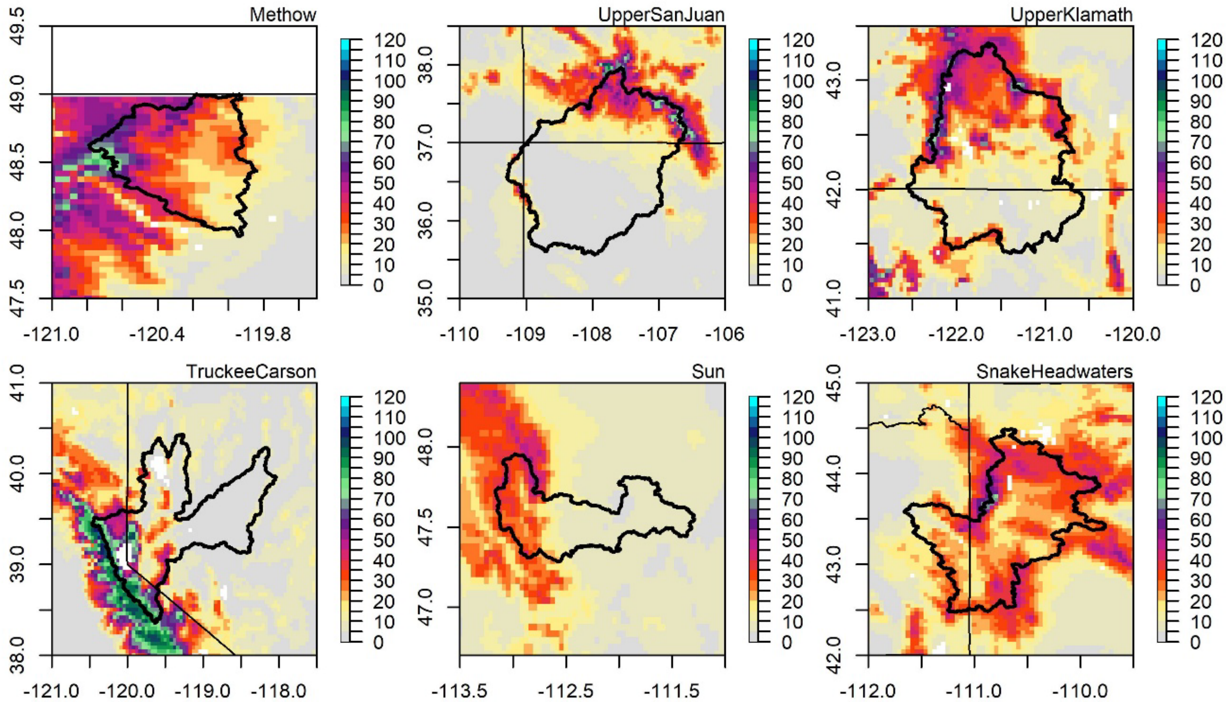

Figure 10.—Average daily snowfall (mm of water) from UA SWE during the top 8 heaviest snowfall events identified in SNOTEL observations between 1982 and 2018. Thin black lines represent state boundaries.

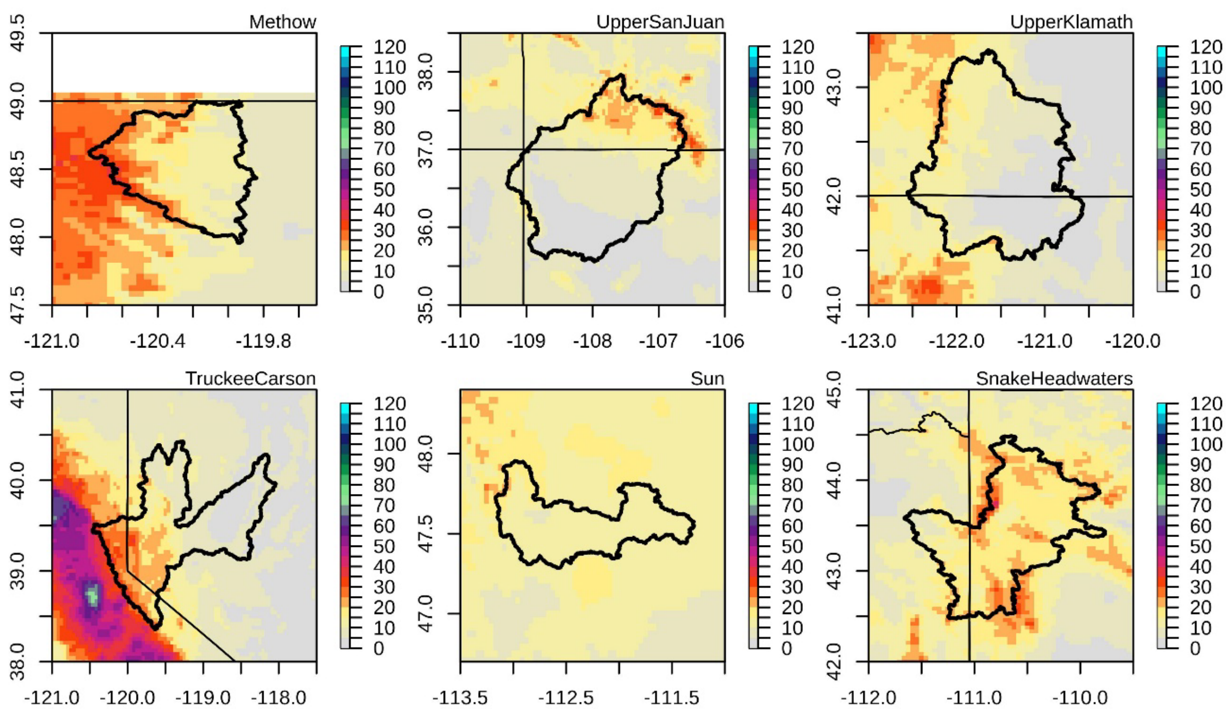

Figure 11.—Average daily precipitation (mm) from PRISM during the top 8 heaviest snowfall events identified in SNOTEL observations between 1982 and 2018. Thin black lines represent state boundaries.

Differences between average UA SWE snowfall and average PRISM precipitation during the top 8 snowfall events identified with point SNOTEL observations are illustrated in figure 12. Grid cell differences between the datasets range from -80 mm to +80 mm, where differences are largest in the two basins where snowfall and precipitation totals are largest: Methow and Truckee-Carson. In general, average snowfall depths from UA SWE are greater than average PRISM precipitation depths in regions of higher elevation. These differences are emphasized in the Truckee-Carson basin and may be related to the treatment of terrain and terrain changes in each algorithm. basin-average differences range from negative (e.g., Upper San Juan) to positive (e.g., Snake Headwaters), indicating that the sign and magnitude of differences between the datasets vary spatially.

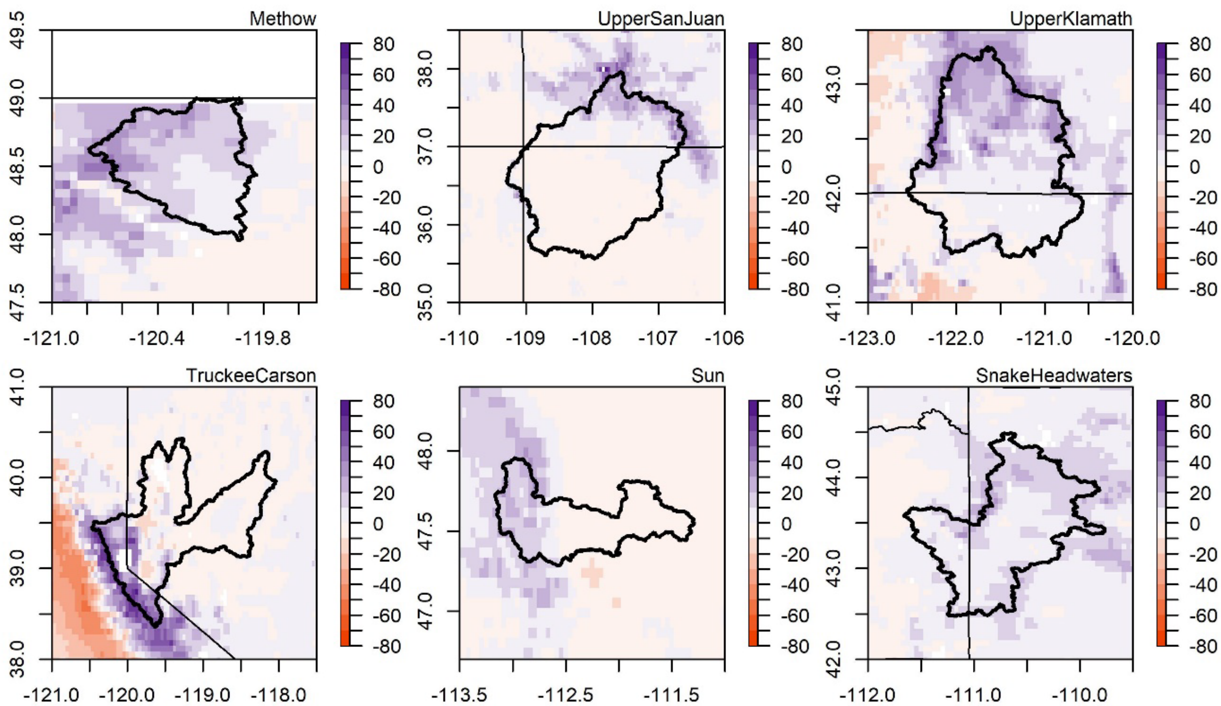

Figure 12.—Average UA snowfall minus PRISM precipitation (mm) during the top 8 heaviest snowfall events identified using SNOTEL observations. Thin black lines represent state boundaries.

Results in figure 12 suggest that UA SWE and PRISM datasets disagree in snowfall and precipitation magnitude during the eight heaviest historical snowfall events. This finding has implications for future hydrologic applications of either dataset, particularly during heavy snowfall events. Future research could explore these differences and possibly others among less extreme days, at longer time scales (e.g., weekly totals), and/or in different geographical regions, including at lower elevations.

Historical Weather Types

Inputs

Inputs to the extreme weather type algorithm include normalized atmospheric variables described in previous sections. Example maps of sea-level pressure, 850 hPa specific humidity, and 500 hPa geopotential height for each of the top eight snowfall events in the Sun River basin are shown in figure 13. These maps represent inputs to the weather typing algorithm and are useful when manually interpreting weather conditions on each of these days. Spatial maps of normalized atmospheric variables for all basins are shown in appendix B.

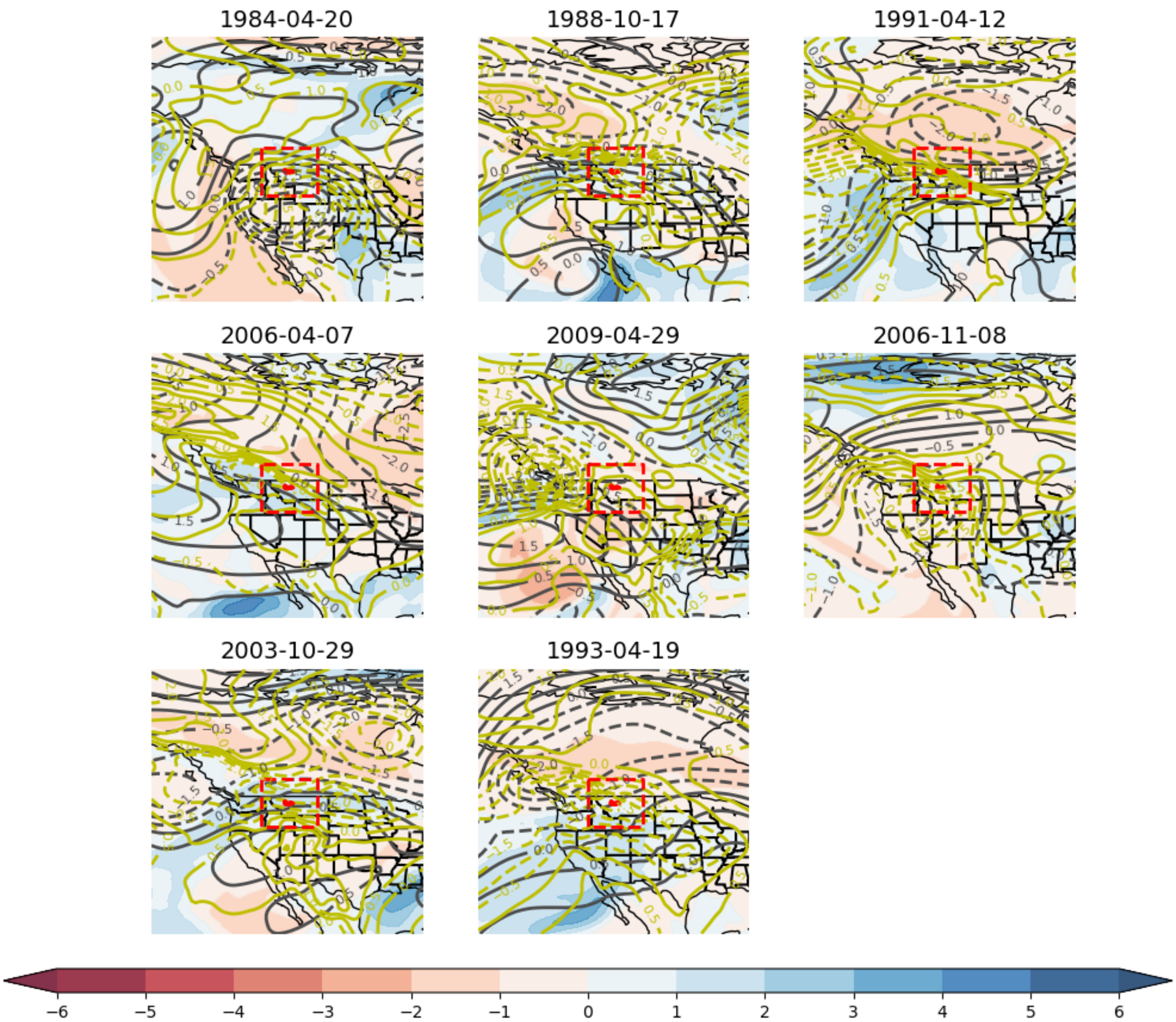

Figure 13.—Anomalous weather conditions for each of the top eight daily snowfall events for the Sun River basin ranked from greatest snowfall total to lowest snowfall total. Shading represents anomalies of 850 hPa specific humidity, dark grey lines represent anomalous 500 hPa geopotential height, and yellow lines represent anomalous sea level pressure.

Outputs

We apply the automated weather typing algorithm of Prein and Mearnes (2021) to cluster weather conditions during the top eight historical heaviest snowfall events in each watershed separately. Average conditions during the days in each weather type are shown in the top plots of each summary figure (e.g., a, b, and c in figure 14 through figure 19), whereas weather type centroids, which represent average conditions among events in each weather type, are shown in the bottom row of each summary figure (e.g., a1, a2, a3 in figure 14 through figure 19). Unless otherwise stated, results from the automated weather typing routine are plotted in the same manner, though the number of resulting weather types vary by basin.

Methow basin

There are two types of weather patterns from the fall through winter that have historically produced extreme snowfall events in the Methow basin (figure 14). The most notable difference between the two weather types is the location of the low-pressure and high-pressure systems with respect to the Methow basin. Both types include four of the eight total events. The first weather type occurs during late fall and early winter. The pattern is dynamically driven by divergence aloft produced from the nose/left-front quadrant of a jet streak over the basin, a vertically stacked low-pressure system off the west coast of British Columbia, and a warm front just south of the basin producing southeasterly winds over the basin which creates orographic lift. All these features produce dynamic lift, as opposed to thermodynamic lift or instability, over the basin. The location of the vertically stacked low-pressure west of the basin allows advection of a moisture plume from the Pacific Ocean over the basin in the form of a possible AR event (referred to as AR-like event).

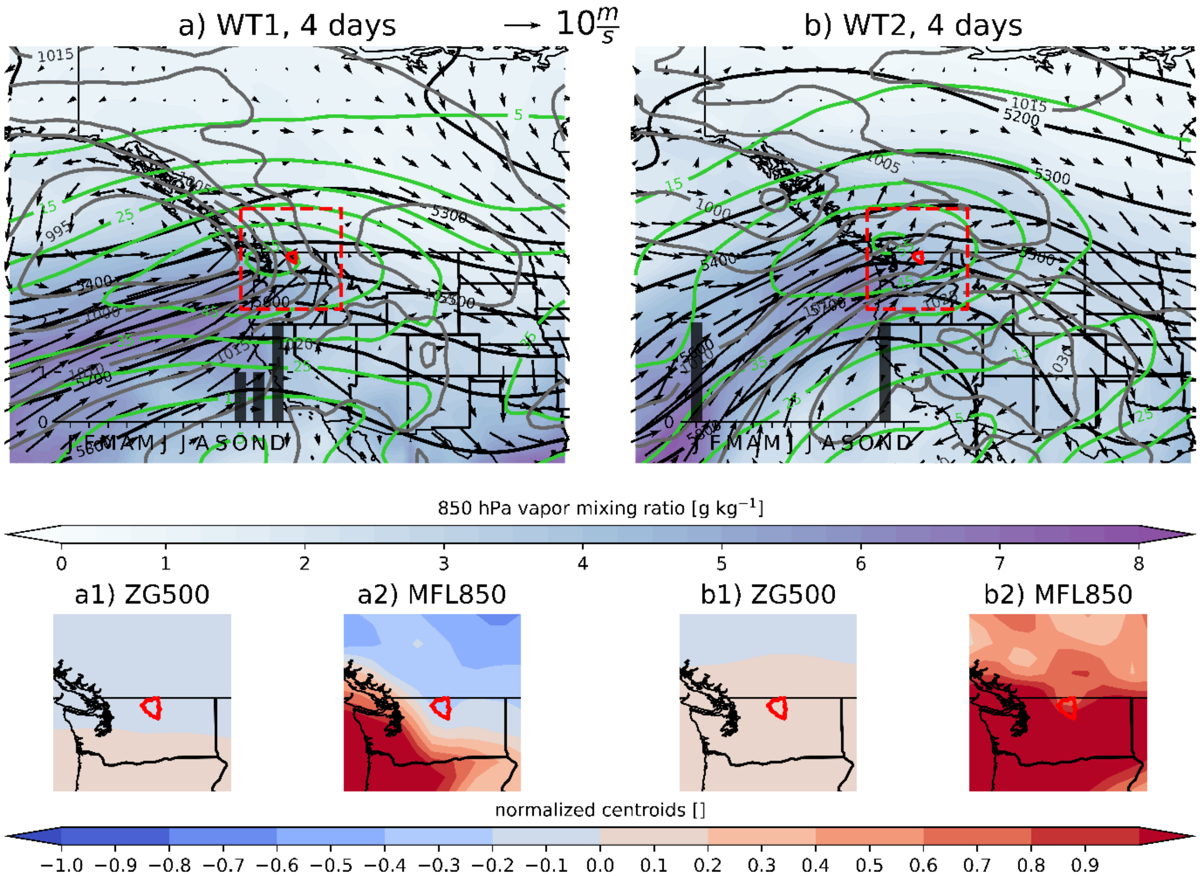

Figure 14.—Weather types that describe the top eight heaviest snowfall events in the Methow basin (top row). Average weather conditions on days in each weather type, where shading represents 850 hPa water vapor (g/kg), black vectors represent 200 hPa horizontal wind speed (m/s), grey contour represent sea-level pressure (hPa), and green contours represent 500 hPa geopotential height (m) (bottom row). Normalized centroids for the variables that define the weather types relevant to snow in the Methow basin. Variable descriptions are listed in table 2. The red polygon shows the drainage area.

The second weather type of interest to the Methow basin occurs during late fall and winter (e.g., November and January). The pattern features a combination of dynamic and thermodynamic forcing mechanisms. Compared to the first weather type, the low- and high-pressure systems are situated more to the north and west relative to the basin. Because of this, the warm front is positioned north of the basin and instability and moisture are more prevalent than with the first weather type. This also means that orographic lift is not as important in this weather type, as there is a southwesterly wind over the basin. Much like the first weather type, a plume of moisture from the Pacific Ocean is advected over the basin due to the placement of the low- and high-pressure systems. This is referred to as an AR-like event.

Snake River basin

The Snake River basin includes three types of weather patterns that produce extreme snowfall events (figure 15). The weather events can occur in the fall and winter and feature mostly dynamic forcing due to jet streaks and shortwaves, orographic lift, and moisture coming from the

Pacific Ocean using preferred moisture pathways through the lower elevation valleys across the Western United States. However, for this basin, the efficient conversion of moisture to precipitation is more important than abundant moisture. Weather types one and two are the most common.

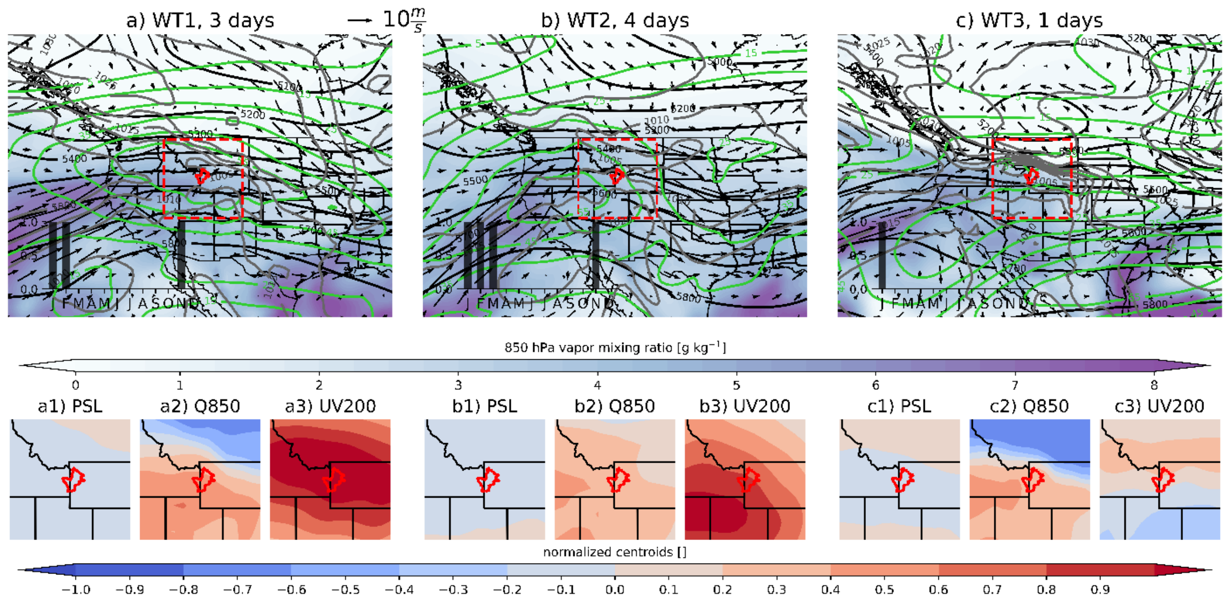

Figure 15.—Same as figure 14, except valid for the Snake River basin.

The first weather type appears during late fall or winter. Some dynamic lift is produced by divergence aloft caused by a strong jet streak over the basin, a cold front north of the basin, and favorable southwest surface winds creating orographic lift. This weather type has the most moisture of the three weather types (seen visibly in the normalized centroid plot in a2) and represents an AR-like event.

The second weather type occurs in late fall, winter, and early spring. The basin is under the left front quadrant and nose of a jet streak and features the strongest upper-level divergence of the three weather types. In contrast to the other two weather types, a frontal boundary does not appear to be near the basin. Rather, it seems that most low-level convergence is being caused by favorable orographic lift. As with the other weather types, efficient use of available moisture is more critical than abundant moisture due to the distance from the moisture source.

The third weather type only occurs in January. The basin is under the right rear quadrant of a modest jet streak with a very strong jet streak located far away over the northern Gulf of Mexico. A very strong Arctic cold front is located just north of the basin and is likely aiding in surface convergence. As with the other two weather types, low-level convergence is being caused by favorable orographic lift over the basin. This weather type features the least amount of moisture likely because it only occurs in January and has a large amount of Arctic air near the basin. We consider this weather type driven by a cold front.

Sun River basin

The Sun River basin historically features three diverse types of weather patterns that produce extreme snowfall events (figure 16). The weather events can occur anytime from fall through spring and feature dynamic and thermodynamic forcing with moisture sources ranging from the Pacific Ocean to the Gulf of Mexico. Weather type one is the most common weather type, which describes four of the eight events (figure 16, bar graph in plot a).

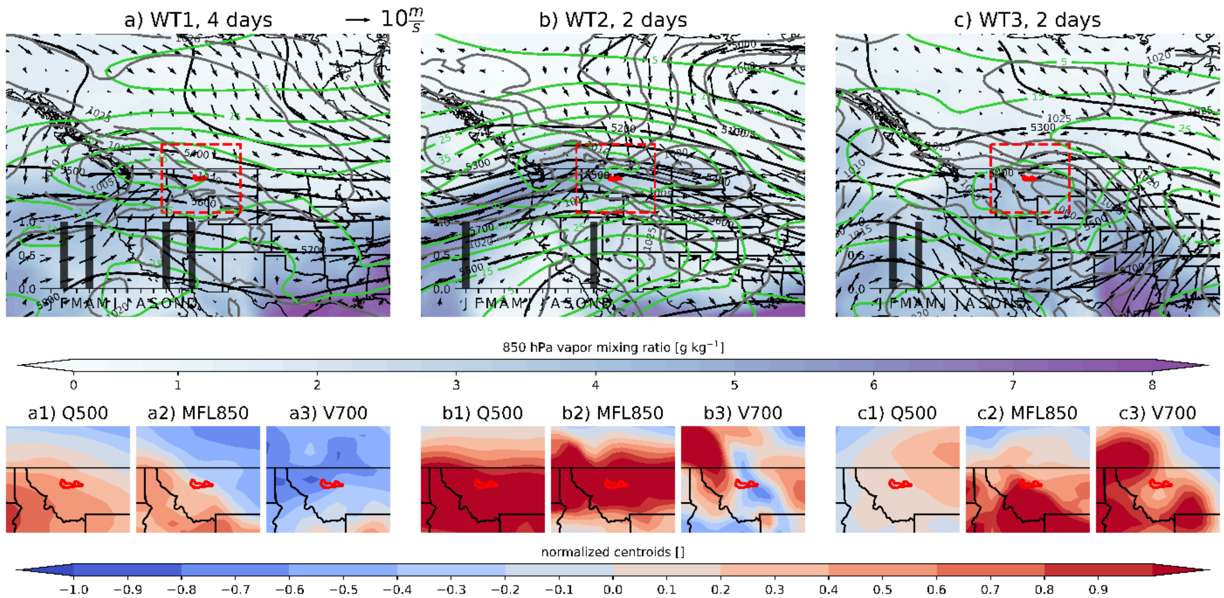

Figure 16.—Same as figure 14, except valid for the Sun River basin.

The first weather type appears between fall into spring (figure 16, plot a). Dynamic lift is produced by divergence aloft caused by the nose of a jet streak (figure 16, green lines) over the basin, a low-pressure system (Figure 16, gray lines and black vectors) near Vancouver Island, and a front (figure 16, gray lines, black vectors) near/over the basin causing surface convergence. Surface moisture (figure 16, shading in plot a and plot a2) is not abundant but middle-level moisture (figure 16, plot a1) is important for this weather type. The dominant mechanisms here is a front.

Late fall and early winter are the seasons when the second weather type occurs (figure 16, plot b). The basin is under the right front quadrant of a jet streak (figure 16, green lines), which typically promotes stability and sinking air. Accordingly, this weather type is driven by deep moisture and surface convergence due to a front (figure 16, gray lines, black vectors) located over the basin rather than upper-level divergence. The deep moisture plume (figure 16, shading in plot b, plots b1 and b2) originates over the Pacific Ocean and may be an inland penetrating Atmospheric River type event. The dominant mechanism here is AR-like.

The third weather type occurs in late winter and spring (figure 16, plot c). This setup is a classic upslope event where air is forced to rise due to topography which results in large amounts of localized precipitation. There is no jet streak (figure 16, green lines) to provide upper-level support for this event. Rather, a strong surface low-pressure system (figure 16, gray lines, black vectors) is located southeast of the basin with a cold front (figure 16, gray lines, black vectors) just south of the basin. The surface low creates a strong easterly surface wind (figure 16, black vectors) near the basin. The main moisture source is the Gulf of Mexico with additional moisture from the Pacific Ocean possible (figure 16, shading in plot c, plots c1 and c2). As the wind travels from the eastern plains of Montana westward, it is forced to rise due to an increase in elevation. Once the wind reaches the abrupt elevation change of the Sawtooth Range in the basin, the orographic effect is increased, and a localized maximum of precipitation is produced.

Truckee-Carson basin

Extreme snowfall episodes have been caused by two distinct types of weather patterns in the Truckee-Carson basin (figure 17). Majority of the events occur during the winter, feature low-pressure near or west of the Pacific Northwest, a jet streak just to the west of the basin, high-pressure off the coast of Baja California, and a deep plume of moisture from the Pacific Ocean coming ashore over north-central California (AR type event). Weather type two occurs more than weather type one among the population of eight events.

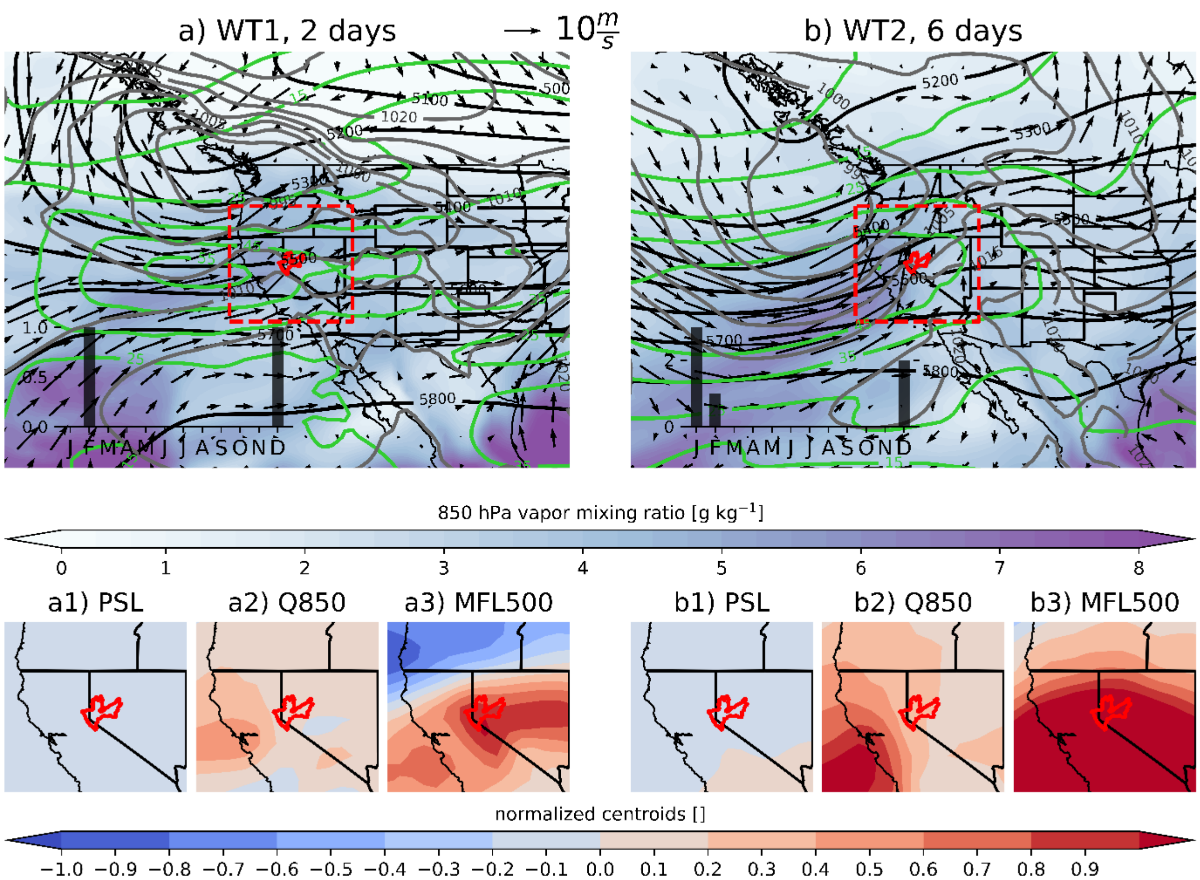

Figure 17.—Same as figure 14, except valid for the Truckee-Carson basins.

The first weather type appears in winter (December and February) and represents an unremarkable AR type event. Dynamic lift is produced by divergence aloft caused by the nose of a strong jet streak approaching the basin and southwest surface winds. Across northern California there is also a deep, but marginal, moisture plume originating from the Pacific Ocean with the best moisture well west of the coast of Baja California and not affecting the basin. There is an arctic cold front near the surface low over Vancouver Island and extending east along the United States-Canadian border. Together, these conditions likely result in available moisture that creates a favorable environment for heavy snowfall within the basin.

The second weather type of interest to the Truckee-Carson basins appears in winter and represents a strong AR type event. Dynamic lift is produced by divergence aloft caused by the nose of a large jet streak and low-level convergence caused by strong southwest and south-southwest surface winds converging over the basin. Across northern California there is also a deep moisture plume originating from the Pacific Ocean. This weather type is large in spatial extent and tends to control the weather over the Western United States. This feature is different from weather type one, which only affects a portion of the Western United States.

Upper Klamath basin

The Upper Klamath basin features three types of weather patterns that produce the top eight historical snowfall events (figure 18). All three of the weather types occur during winter, specifically December and January, and feature low-pressure centers over the Gulf of Alaska, high-pressure centers off the coast of southern California, and a plume of moisture from the Pacific Ocean coming ashore over northern California into southern Oregon. Weather type one includes two days, whereas weather types two and three each include three days.

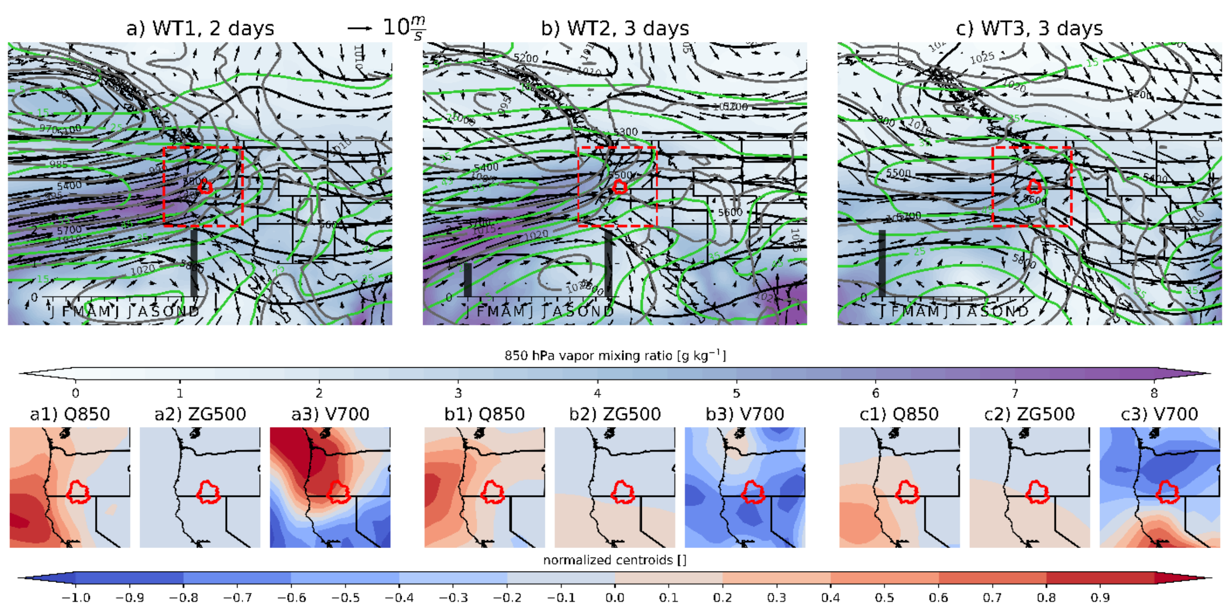

Figure 18.—Same as figure 14, except valid for the Upper Klamath basin.

The first weather type of interest to the Upper Klamath basin appears in the early winter. Dynamic lift is produced by divergence aloft caused by the nose of a strong jet streak approaching the basin. Strong onshore surface winds are caused by a sharp surface pressure gradient between an intense surface low-pressure over the Gulf of Alaska (akin to a weak category three hurricane) and high-pressure off the coast of Baja California. From northern California into southern Oregon, there is also a deep moisture plume originating from the Pacific Ocean. The upper-level trough is negatively tilted providing some thermodynamic instability over the basin. This weather type is likely an AR type event. Warm, humid air from the Pacific Ocean is brought inland, raising the Upper Klamath basin's rain-to-snow transition zone. Since most of the basin is below 5,000 feet in elevation, it is possible that heavy snowfall happens predominately at higher elevations. The warm humid air may transport vast amounts of moisture inland, but that moisture may not result in extreme snowfall events. There is a surface low and a mid-level shortwave across the eastern Dakotas/western Minnesota.

The second weather type relevant to the Upper Klamath basin also occurs during winter. The pattern is similar to the first weather type except all components are weaker. The upper-level trough has a slight negative-tilt which introduces a limited amount of thermodynamic instability. In contrast to type one, there is a shortwave across Baja California and mostly zonal flow across the Great Plains. The dominant mechanism is AR-like.

The third weather type also occurs in winter. The pattern is similar to the first and second weather types, albeit weaker. This type features a neutrally tilted upper-level trough which removes the thermodynamic instability of the first type. There may be a cold front located near the basin which provides most of the lift for this weather type. This is important as the dynamics, thermodynamics, and moisture content of this weather type are unremarkable. Similar to type one, there is an upper-level shortwave over the Great Plains. We refer to this mechanism as a cold front.

Upper San Juan basin

There are two types of weather patterns that produce the top eight snowfall events in the Upper San Juan basin (figure 19). The weather events occur in the fall and winter and feature modest dynamic forcing due to jet streaks and shortwaves, with orographic lift combined with surface speed convergence likely playing a key role, and moisture coming from the Pacific Ocean in the lower levels and possible from the Gulf of Mexico in the mid-to-upper levels in weather type two. Surface fronts are not as critical for this basin when compared to the other basins due to the high elevations of the San Juan Mountains. Weather type one more common than weather type two.

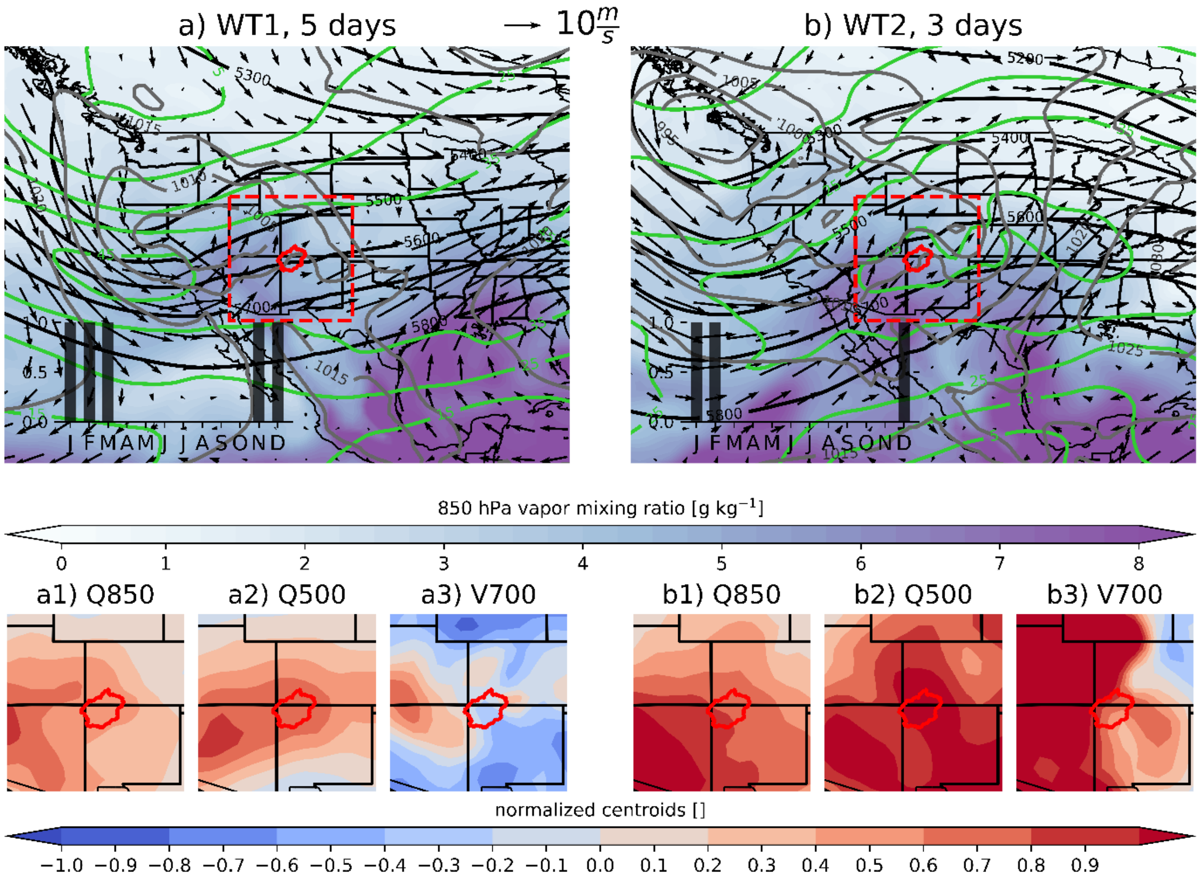

Figure 19.—Same as figure 14, except valid for the Upper San Juan basin.

The first weather type appears during the fall, throughout the winter, and in early spring. Results suggest that some dynamic lift is produced by divergence aloft caused by the nose of a modest jet streak approaching the basin, with relatively deep Pacific moisture, and favorable southwest surface winds creating orographic lift. This weather type likely only includes Pacific moisture due to the position of high pressure farther east and south over the Gulf of Mexico as compared to weather type two. We label the dominant mechanism an upper-level trough.

The second weather type only appears during the winter. Modest dynamic lift is produced by a jet streak over the basin. Low-level moisture is from the Pacific Ocean, but mid-to-upper-level moisture is likely from the Gulf of Mexico. High pressure is centered over the northern Gulf of Mexico which is advecting surface moisture into parts of Texas and mid-to-upper-level moisture into New Mexico and southwest Colorado. This weather type has substantially more moisture than the previous one because there are two moisture sources present. As with the first weather type, we consider the dominant mechanism an upper-level trough.

Large Ensemble Output

Historical Conditions

We present comparisons between simulated atmospheric fields from the CESM2 LENS2 ensemble and ERA-Interim prior to discussing findings from the simulated weather type analysis. We use these comparisons to characterize differences between these two datasets during the historical period when reanalysis data are available. We focus on atmospheric variables identified and utilized in the historical extreme weather typing algorithm. Climatological differences between average daily October through April conditions averaged over all 10 LENS2 members and ERA-Interim between 1982 and 2018 (for a total of 38 years) are shown in figure 20.

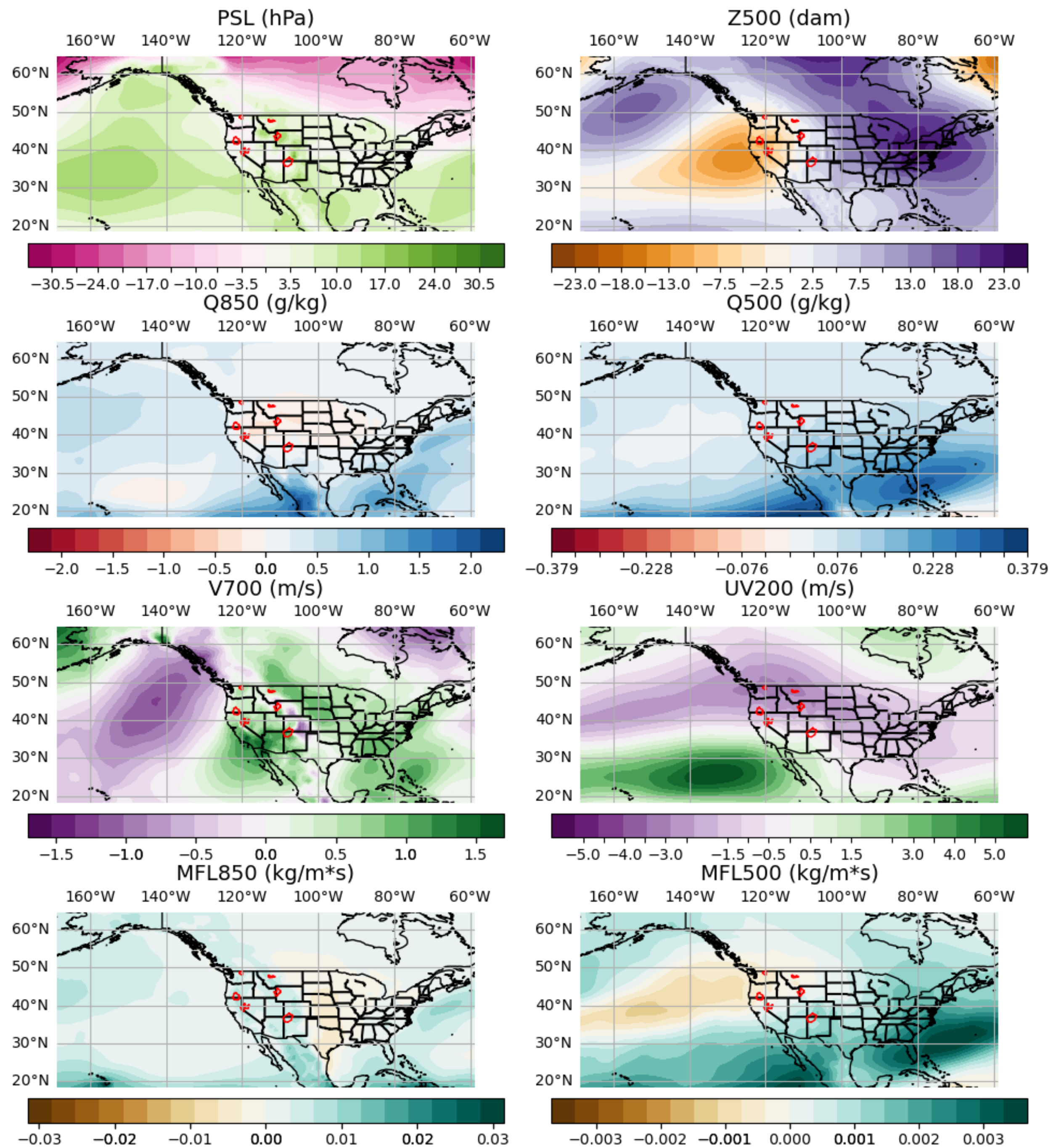

Figure 20.—Difference in average cool-season daily (left to right, top to bottom) sea-level pressure (PSL; hPa), geopotential height at 500 hPa (Z500; dam), specific humidity at 850 hPa (Q850; g/kg), specific humidity at 500 hPa (Q500; g/kg), meridional wind speed at 700 hPa (V700; m/s), horizontal wind speed at 200 hPa (UV200; m/s), moisture flux at 850 hPa (MFL850; kg/ms), and moisture flux at 500 hPa (MFL500; kg/ms) between 1982 and 2018 between CESM2 LENS2 ensemble mean and ERA-Interim (computed as CESM2 LENS2-ERA-Interim).

Results show that on average, during the cool-season, sea level pressure in CESM2 LENS2 is similar to slightly higher across much of the United States compared to ERA-I. Positive differences are largest over the eastern Pacific Ocean. Differences in 500 hPa geopotential height show three primary action centers over the domain in figure 20. Specifically, 500 hPa geopotential heights are higher in CESM2 LENS2 over the Aleutain Low, most of Canada, and the eastern half of the United States. Off the west coast of California, 500 hPa geopotential heights in CESM2 LENS2 are lower than ERA-Interim. Cool-season differences in specific humidity between the CESM2 LENS2 ensemble and ERA-Interim at 850 hPa and 500 hPa are largest over the southernmost latitudes in the domain, with particular emphasis over water (Pacific and Gulf of Mexico). Differences are slightly negative over CONUS at 850 hPa, a signal that is not present at 500 hPa.

The difference field in meridional wind speeds at 700 hPa shows a wave-like feature over the domain, with negative differences over the eastern North Pacific, positive differences off and over southern California and Arizona, positive differences over parts of Canada, and negative differences across much of the eastern United States and Puerto Rico. Horizontal wind speeds at 200 hPa show a large dipole pattern over the eastern north Pacific Ocean, with positive differences located largely north of the 40°N latitude band and negative differences between 20°N and 30°N.

Projected Changes

We present projected changes in atmospheric variables relevant to the historical weather typing analysis to document the average change signal between historical and future conditions. Projected changes between average future CESM2 LENS2 conditions and average historical CESM2 LENS2 conditions (all valid using October through April days) are shown in figure 21.

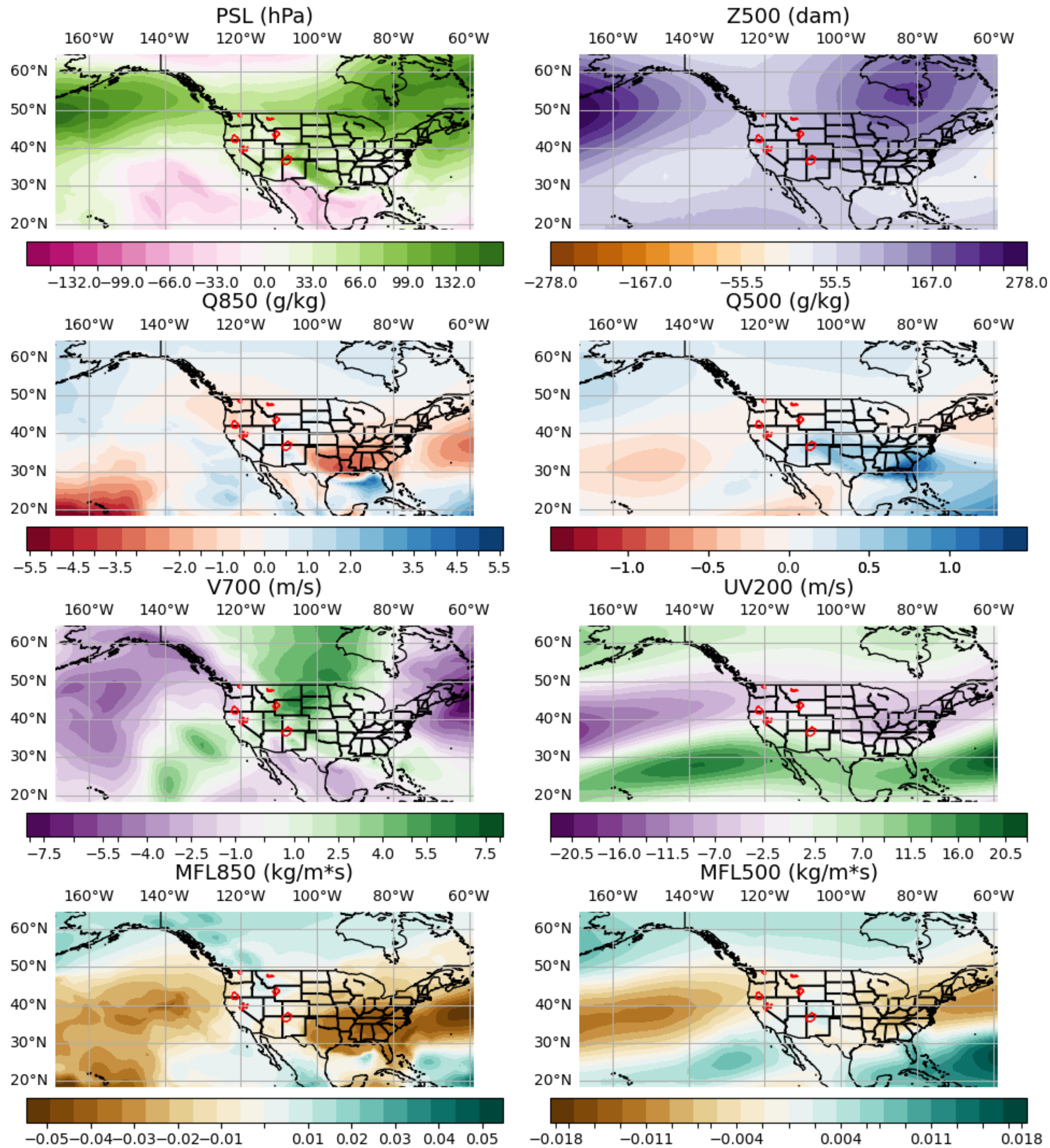

Figure 21.—Difference in average cool-season (Oct-Apr) daily (left to right, top to bottom) sea-level pressure (PSL; hPa), specific humidity at 850 hPa (Q850; g/kg), specific humidity at 500 hPa (Q500; g/kg), geopotential height at 500 hPa (Z500; dam), meridional wind speed at 700 hPa (V700; m/s), horizontal wind speed at 200 hPa (UV200; m/s), moisture flux at 850 hPa (MFL850; kg/ms), and moisture flux at 500 hPa (MFL500; kg/ms) between historical (1980–2018) and future (2062–2098) CESM2 LENS2 ensemble means (computed as future minus historical).

Results in figure 21 show differences in long-term average conditions projected by the CESM2 LENS2 ensemble members during the cool season (October 1 through April 30). The sea-level pressure map shows large projected increases over most of the continental United States (CONUS) and extending in eastern Canada. There are large increases projected over the Aleutian Islands. Finally, there are projected decreases in sea-level pressure over northwestern Canada (near the border with Alaska), Mexico, and parts of the eastern North Pacific. These projected changes disagree in sign with projected changes in all season sea-level pressure from a Coupled Model Intercomparison Project Phase 5 (CMIP5) multi-model ensemble presented in Knutson and Ploshay (2021). See Knutson and Ploshay (2021) for their list of models. The CESM2 LENS2 projected changes in sea level pressure also disagree in sign with projected winter changes in sea-level pressure from Manzini et al. (2014).

Geopotential height at 500hPa is projected to increase across almost the entire domain shown in figure 21. There are two clear action centers with the largest positive changes located off the southwest coast of Alaska and near the southern lobe of Hudson Bay (near the border between Ontario province and Quebec province). These cool-season changes in 500 hPa geopotential height agree with the sign of simulated historical trends from CMIP5 models presented in Christidis and Stott (2016). They also agree in sign with multi-model projected changes in autumn (September, October, November) 500 hPa geopotential heights from Knutson and Ployshay (2021).

Spatial maps of projected changes in 850 hPa and 500 hPa moisture show differing patterns. At 850 hPa, the largest decreases are projected over the southern eastern Pacific Ocean and along the southeastern coast of the United States. There are also negative projected changes off the east coast of the United States, in the western Atlantic Ocean. At 500 hPa, there is slightly more spatial homogeneity in projected changes. There are negative changes projected over parts of the eastern Pacific Ocean, extending over parts of the Pacific Northwest. There are positive changes projected over the southeastern United States, extending over the western Atlantic Ocean.

Projected changes in 700 hPa meridional winds show large decreases (i.e., mean meridional winds are projected to become more northerly) near the southern shore of Alaska, over the west coast of Canda, and off the east coast of the United States. In the central portion of North America, mean meridional winds are projected to become more positive (i.e., projected to become more southerly). Projected changes in 200 hPa horizontal wind speeds show positive changes largely between 30°N and 50°N across much of the domain in figure 21. Large negative changes are projected to occur largely between 20°N and 30°N (with some changes projected north of 30°N) across much of the domain. Projected changes in 200 hPa horizontal wind speed are also negative north of 50°N. Projected changes in 200 hPa horizontal wind speeds computed here resemble the multi-model winter (December, January, February) change signal at 250 hPa from CMIP5 models presented in Harvey et al. (2020), particularly their figure 3d.

Mean cool season changes in moisture flux at 850 hPa and 500 hPa are shown in the bottom two plots of figure 21. At 850 hPa, the CESM2 LENS2 ensembles project negative changes in moisture flux over the eastern North Pacific, over the southeastern United States, and off the coast of eastern United States (over the western Atlantic Ocean). The ensemble projects increasing moisture flux over most of Canada. At 500 hPa, moisture flux is projected to decrease over parts of the eastern Pacific Ocean, largely between 30°N and 50°N. Decreases are also projected over the eastern United States and off the coast. Projected increases in moisture flux are located over most of Canada, off the western coast of the Baja Peninsula, and over the western Atlantic Ocean between 20°N and 30°N.

Mapping to Weather Types

For each basin, we map every simulated day between October 1 and April 30 during the historical (1982–2018) and future (2062–2098) periods to each possible weather type (up to three, depending on basin) and record Euclidean Distance (ED) and Manhattan Distance (MD). The weather type with the lowest MD or the lowest ED is considered the winning (or closest) weather type for each respective metric. Distributions of historical and future MD and ED for each basin among all CESM2 LENS2 ensemble member are shown in figure 22. These plots demonstrate the impact of metric in mapping each day to a weather type. For example, applying the MD metric to select a best-fitting weather type results in two of two weather types being selected in the Methow basin during both historical and future periods. Conversely, applying the ED metric to select a best fitting weather type in the Methow basin results in all days from all ensemble members during the historical and future periods being mapped to one of two possible weather types. Results for the Snake River basin in figure 22 show a similar finding in that there are fewer best matching weather types identified with ED than with MD among all CESM2 LENS2 ensemble members during the historical and future periods. In the Truckee-Carson and Upper San Juan basins, both metrics map all days to a single weather type. Conversely, in the Sun and Upper Klamath basins, simulated days are mapped to all three weather types using both MD and ED.

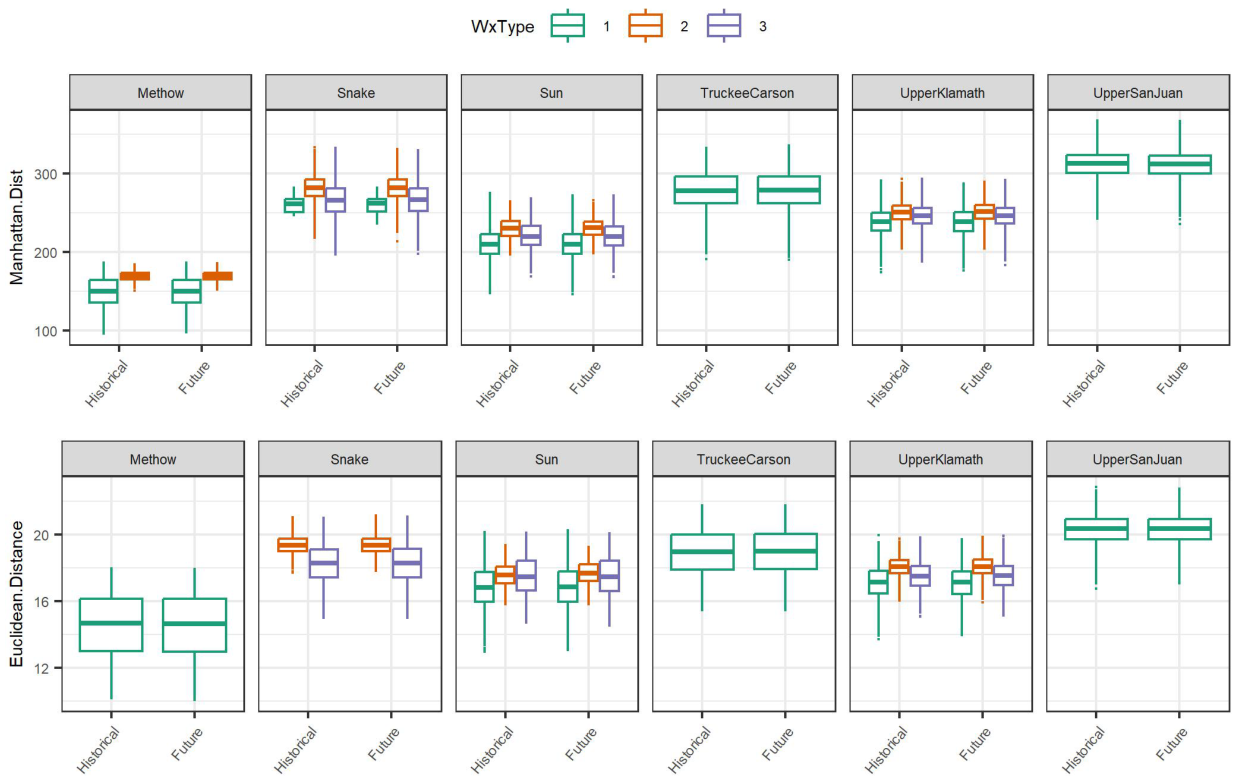

Figure 22.—Box and whisker plots of (top) Manhattan Distance and (bottom) Euclidean Distance for all cool-season days during the historical and future periods among all CESM2 LENS2 ensemble members colored by best fit historical weather type for each basin.

Results in figure 22 suggest that identifying the best matching weather type with MD provides improved distinction among the possible weather types. Consequently, we present an analysis of the top eight weather types based on lowest MD during the historical and future periods for each CESM2 LENS2 member. Results are shown in figure 23. Plots in figure 23 show the number of top eight days identified with MD that map to each possible weather type for each ensemble member in each basin. These results corroborate findings in figure 22, showing that best matching events (e.g., lowest MD) in the Methow, Sun, Truckee-Carson, and Upper San Juan basins map to weather type 1. The top eight events in the Snake River basin map to weather type 3. Finally, the top eight events in the Upper Klamath basin map to weather types 1 and 3 during the historical and future periods. Upper Klamath basin is the only basin where the top eight events map to more than one weather type, a finding that is true during the historical and future periods.

Figure 23.—Number of top eight events that map to each weather type based on Manhattan Distance during the (top) historical and (bottom) future periods for each CESM2 LENS2 ensemble in each basin.

We further characterize the top eight events among ensemble members plotted in figure 23 by examining the simulated month of occurrence. Specifically, bars in figure 24 show number of top eight events from all ensemble members (maximum count of eight events times 10 ensemble members equals 80 total events) that occur in each month during the historical and future time periods. We see that the top eight events (as identified from the MD metric) occur during almost all cool-season months, contrary to the observed timing summarized in the previous section (see barplots in figure 14 through figure 19). In the Methow basin, historical events occur between October and April, with the largest number of events occurring during April. This finding is also true in the Methow basin during the future period. In the Snake basin, historical events occur during all months (October through April), with the largest number occurring during November and December. During the future period, December stands out as the month with the largest number of events. In the Sun basin, historical events occur during November through April, while future events occur during October through April. Historical events in the Truckee-Caron basins occur between October and April, with January having the largest number of events among months. In the future period, November and December have the largest number of events. Upper Klamath basin has top eight events that map to weather type one and three during the historical and future periods, where weather type one shows up more often than weather type three. Top eight events occur most during February and March during the historical and future periods, respectively. In the Upper San Juan basin, historical events occur most often during April. In the future period, events occur most often during November. Weather type two is not selected among all basins. Ensembles produce the top eight events during all months included in the analysis (October through April) in all basins except the Sun basin. This finding could be related to sample size, which is much larger here than in the historical observed analysis (population size of eight events in all basins as opposed to 80 in simulated events).

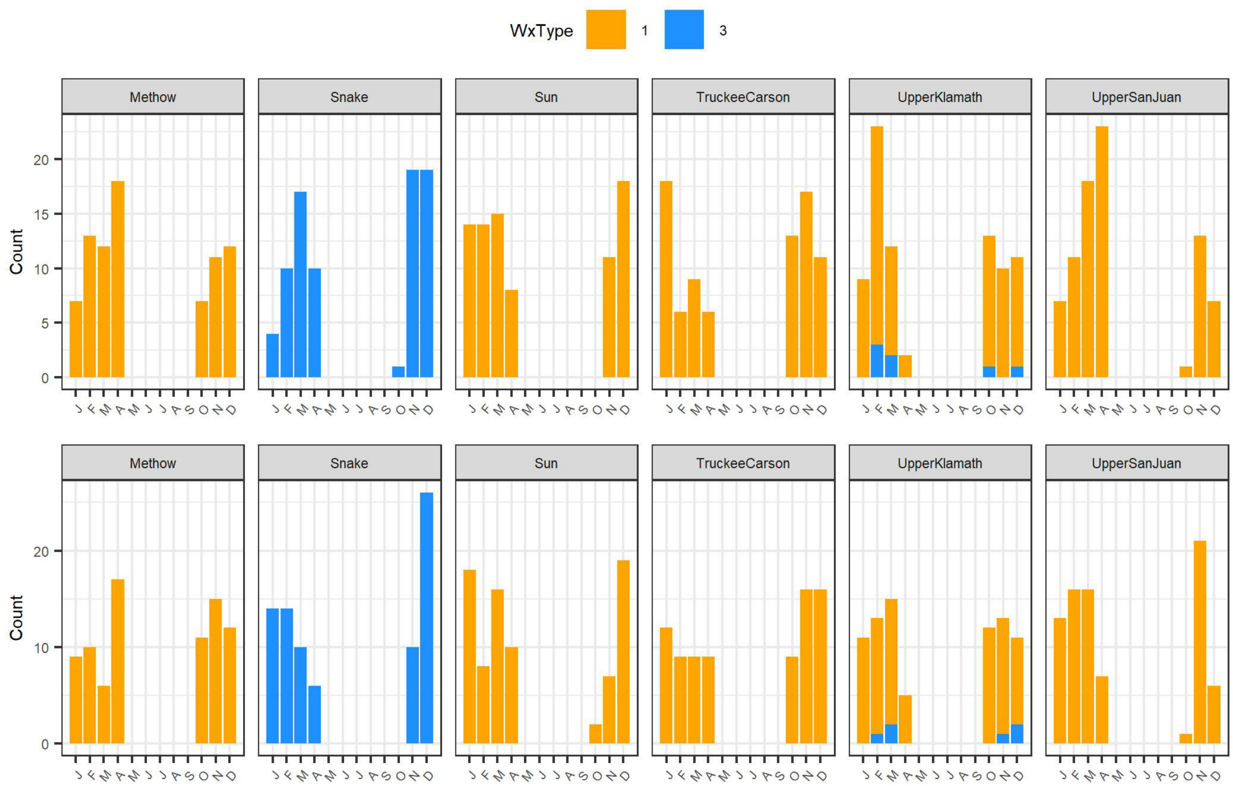

Figure 24.—Number of top eight days identified by the lowest Manhattan Distance simulated among all CESM2 LENS2 ensemble members that occur during each month in the (top) historical and (bottom) future periods.

Conclusions

Seasonal snowpack is a critical resource for water management across many parts of the world, including the western United States. In this study, we aim to improve understanding of snowfall events across the Western United States by exploring historical snowfall events at point SNOTEL stations, characterizing weather types associated with the top eight heaviest historical snowfall events, and exploring simulation of historical weather types in climate projections. We focus on six Reclamation watersheds located in headwater regions, which include the Methow basin, WA, the Sun River basin, MT, the Upper Snake River basin, ID/WY, the Upper Klamath Lake basin, OR/CA, the Truckee-Carson basins, CA/NV, and the Upper San Juan basin, UT/AZ/CO/NM. Each of these basins is differentiated from the others by unique historical snowfall events and weather patterns associated with heavy snowfall events.

We quantify the number of days per water year with positive snowfall totals, maximum daily snowfall total per water year, and water year total snowfall among a subset of SNOTEL stations. Results suggest that the number of snowfall days is greatest in the Methow and Upper Klamath Lake basins, although annual water year total snowfall is often greatest in the Methow and Truckee-Carson basins. Water year maximum daily snowfall varies by SNOTEL station, where some of the largest daily totals are found at stations in the Upper San Juan and Truckee-Carson basins.

We investigate weather types associated with the eight heaviest historical snowfall events in each basin using the weather typing algorithm of Prein and Mearns (2021), where the number of weather types (e.g., clusters) varies by basin. Finally, we document how average atmospheric conditions from ten CESM2 LENS2 ensemble members compare with weather types identified with the ERA-Interim dataset. We map historical and future cool-season days from the ensemble members to historical weather types to explore possible changes in seasonality. The large ensemble provides a larger population size to examine timing of events. Collectively, these analyses support the characterization of historical heavy snowfall events across six Reclamation basins located in headwater regions using reanalysis and model simulations.

Overall, results show that two dominant weather types explain the historical heavy snowfall events in the Methow, Truckee-Carson, and Upper San Juan basins. Conversely, three weather types best describe forcing of the historical heavy snowfall events in the Snake, Sun, and Upper Klamath Lake basins. AR events play a role in five of the six basins, emphasizing the importance of this mechanism to snowfall beyond the West Coast (Swales et al. 2016). Other forcing mechanisms like fronts and upper-level troughs are also important to heavy snowfall events in the basins of interest to this study. Results from this study are important because we document a clear relationship between atmospheric forcing mechanisms and heavy snowfall events in headwater basins across Reclamation's management domain. We show that forcing mechanisms vary spatially and temporally, although AR-like events are important in many regions. Water managers can use this information to identify clear weather types to pay particular attention to during the winter seasons. This study also provides information on weather types of interest to snowfall for climate change studies.

Future research may explore air temperatures during historical heavy snowfall events and the association with differing weather types. Perhaps there is a relationship between weather type, the rain/snow line, and accumulated snowfall. Future studies may also explore how the mechanisms identified in this study may change in the future, including seasonality, magnitudes, and frequency.

References

Bengtsson, L., S. Hagemann, and K.I. Hodges. 2004. Can climate trends be calculated from reanalysis data? *Journal of Geophysical Research: Atmospheres* 109(D11).

Bholowalia, P. and A. Kumar. 2014. EBK-Means: A Clustering Technique based on Elbow Method and K-Means in WSN. *International Journal of Computer Applications* 105(9): 17–19.

Broxton, P.D., N. Dawson, and X. Zeng. 2016a. Linking snowfall and snow accumulation to generate spatial maps of SWE and snow depth. *Earth and Space Science* 3(6): 246–256.

_____. 2016b. Why do global reanalyses and land data assimilation products underestimate snow water equivalent?. *Journal of Hydrometeorology*, 17(11): 2743–2761.

_____. 2019. Daily 4 km Gridded SWE and Snow Depth from Assimilated In-Situ and Modeled Data over the Conterminous US, Version 1.

Broxton, P. D., W.J. van Leeuwen, B.M. Svoma, J. Walter, and J.A. Biederman. 2023. Subseasonal to seasonal streamflow forecasting in a semiarid watershed. *JAWRA Journal of the American Water Resources Association* 59(6): 1493–1510.

Bureau of Reclamation (Reclamation). 2021. Emerging Technologies in Snow Monitoring Report to Congress. https://www.usbr.gov/research/docs/news/Emerging_Snow_Monitoring_Report_508.pdf.

Chen, J., F.P. Brissette, and H. Chen. 2018. Using reanalysis-driven regional climate model outputs for hydrology modelling. *Hydrological Processes* 32(19): 3019–3031.

Christidis, N., and P.A. Stott. 2015. Changes in the geopotential height at 500 hPa under the influence of external climatic forcings. *Geophysical Research Letters* 42(10): 798–10,806. doi:10.1002/2015GL066669.

Cook, J. and V. Ramadas. 2020. When to consult precision-recall curves. *The Stata Journal* 20(1): 131–148.

Daly, C., R.P. Neilson, and D.L. Phillips. 1994. A statistical-topographic model for mapping climatological precipitation over mountainous terrain. *Journal of Applied Meteorology and Climatology* 33(2): 140–158.

Danabasoglu, G., J.F. Lamarque, J. Bacmeister, D.A. Bailey, A.K. DuVivier, J. Edwards, L.K. Emmons, J. Fasullo, R. Garcia, A. Gettelman, and C. Hannay. 2020. The community earth system model version 2 (CESM2). *Journal of Advances in Modeling Earth Systems* 12(2): p.e2019MS001916.

Dee, D.P., S.M. Uppala, A.J. Simmons, P. Berrisford, P. Poli, S. Kobayashi, and F. Vitart. 2011. The ERA-Interim reanalysis: Configuration and performance of the data assimilation system. *Quarterly Journal of the Royal Meteorological Society* 137(656): 553–597.

European Centre for Medium-Range Weather Forecasts (ECMWF). ECMWF Reanalysis v5 (ERA5). https://www.ecmwf.int/en/forecasts/dataset/ecmwf-reanalysis-v5 (Accessed 29 Sept. 2023)

Eyring, V., S. Bony, G.A. Meehl, C.A. Senior, B. Stevens, R.J. Stouffer, and K.E. Taylor. 2016. Overview of the Coupled Model Intercomparison Project Phase 6 (CMIP6) experimental design and organization. *Geosci. Model Dev*. 9: 1937–1958.

Fleming, S.W., L. Zukiewicz, M.L. Strobel, H. Hofman, and A.G. Goodbody. 2023. SNOTEL, the soil climate analysis network, and water supply forecasting at the natural resources conservation service: Past, present, and future. *Journal of the American Water Resources Association (JAWRA)* 59(4): 585–599.

Hale, K.E., K.N. Musselman, A.J. Newman, B. Livneh, and N.P. Molotch, (2023). Effects of snow water storage on hydrologic partitioning across the mountainous, western United States. *Water Resources Research* 59(8): e2023WR034690.

Harvey, B.J., P. Cook, L.C. Shaffrey, and R. Schiemann. 2020. The response of the northern hemisphere storm tracks and jet streams to climate change in the CMIP3, CMIP5, and CMIP6 climate models. *Journal of Geophysical Research: Atmospheres* 125: e2020JD032701. https://doi.org/10.1029/2020JD032701

Hersbach, H., B. Bell, P. Berrisford, S. Hirahara, A. Horányi, J. Muñoz-Sabater, J. Nicolas, C.Peubey, R. Radu, D. Schepers, and A. Simmons. 2020. The ERA5 global reanalysis. *Quarterly Journal of the Royal Meteorological Society* 146(730): 1999–2049.

Huning, L.S. and S.A.Margulis. 2017. Climatology of seasonal snowfall accumulation across the Sierra Nevada (USA): Accumulation rates, distributions, and variability. *Water Resources Research* 53(7): 6033–6049.

Isaksen, L., M. Bonavita, R. Buizza, M. Fisher, J. Haseler, M. Leutbecher, and L. Raynaud 2010. Ensemble of data assimilations at ECMWF. Research Department. Meteo-France. https://www.ecmwf.int/sites/default/files/elibrary/2010/10125-ensemble-data-assimilations-ecmwf.pdf

Kay, J.E., C. Deser, A. Phillips, A. Mai, C. Hannay, G. Strand, and M. Vertenstein. 2015. The Community Earth System Model (CESM) large ensemble project: A community resource for studying climate change in the presence of internal climate variability. *Bulletin of the American Meteorological Society* 96(8): 1333–1349.

Knutson, T.R. and J. Ploshay. 2021. Sea level pressure trends: Model-based assessment of detection, attribution, and consistency with CMIP5 historical simulations. *Journal of Climate* 34(1): 327–346.

Lute, A.C. and J.T. Abatzoglou. 2014. Role of extreme snowfall events in interannual variability of snowfall accumulation in the western United States. *Water Resources Research* 50(4): 2874–2888.

Mahto, S.S. and V. Mishra. 2019. Does ERA-5 outperform other reanalysis products for hydrologic applications in India? *Journal of Geophysical Research: Atmospheres* 124: 9423–9441. https://doi.org/10.1029/2019JD031155

Mankin, J.S., F. Lehner, S. Coats, and K.A. McKinnon2020. The value of initial condition large ensembles to robust adaptation decision-making. *Earth's Future* 8(10): e2012EF001610.

Manzini, E., A. Yu. Karpechko, J. Anstey, et al. 2014. Northern winter climate change: Assessment of uncertainty in CMIP5 projections related to stratosphere-troposphere coupling. *Journal of Geophysical Research-Atmosphere.* 119: 7979–7998. doi:10.1002/2013JD021403.

Miller, J.E. 1948. Forecasting the Weather: East Coast Storms. *Weatherwise* 1(2): 36–38.

Milligan, G.W. and M.C. Cooper. 1988. A study of standardization of variables in cluster analysis. *Journal of Classification* 5: 181–204.

National Aeronautics and Space Administration (NASA). National Snow and Ice Data Center Distributed Active Archive Center. Boulder, Colorado https://doi.org/10.5067/0GGPB220EX6A. (Accessed on January 2022).

National Center for Atmospheric Research. 2023. PRISM High-Resolution Spatial Climate Data for the United States: Max/min temp, dewpoint, precipitation [Online]. https://climatedataguide.ucar.edu/climate-data/prism-high-resolution-spatial-climate-data-united-states-maxmin-temp-dewpoint. (Accessed 29 Sept. 2023)

National Snow and Ice Data Center. Daily 4 km Gridded SWE and Snow Depth from Assimilated In-Situ and Modeled Data over the Conterminous US, Version 1 [Online]. https://nsidc.org/data/nsidc-0719/versions/1 (Accessed 29 Sept. 2023)

New Mexico Water Data. SnowView Webmap [Online]. https://catalog.newmexicowaterdata.org/dataset/snowview-webmap (Accessed 29 Sept. 2023).

Nguyen, H., R. Mehrotra, and A.Sharma. 2017. Can the variability in precipitation simulations across GCMs be reduced through sensible bias correction? *Climate Dynamics* 49: 3257–3275.

Oregon State University. 2022. Descriptions of PRISM Spatial Climate Datasets for the Conterminous United States [Online]. https://prism.oregonstate.edu/documents/PRISM_datasets.pdf (Accessed 29 Sept. 2023)

Prein, A.F., G.J. Holland, R.M. Rasmussen, M.P. Clark, and M.R. Tye. 2016. Running dry: The US Southwest's drift into a drier climate state. *Geophysical Research Letters* 43(3): 1272–1279.

Prein, A.F. and L.O. Mearns. 2021. US extreme precipitation weather types increased in frequency during the 20th century. *Journal of Geophysical Research: Atmospheres* 126(7): p.e2020JD034287.

Qi J., Y. Yu, L. Wang, J. Liu, and Y.Wang. 2017. An effective and efficient hierarchical K-means clustering algorithm. *International Journal of Distributed Sensor Networks* 13(8): 1–17.

Rosset, S. July 2004. Model selection via the AUC. *In Proceedings of the Twenty-first International Conference on Machine learning*: 89. July 4–9, 2004. Banff, Alberta, Canada.

Schiemann, R., and C. Frei. 2010. How to quantify the resolution of surface climate by circulation types: An example for Alpine precipitation. *Physics and Chemistry of the Earth, Parts A/B/C*, *35*(9-12): 403–410.

Simpson, I.R., J. Bacmeister, R.B. Neale, C. Hannay, A. Gettelman, R.R. Garcia, et al. 2020. An evaluation of the large-scale atmospheric circulation and its variability in CESM2 and other CMIP models. *Journal of Geophysical Research: Atmospheres* 125: e2020JD032835. https://doi.org/10.1029/2020JD032835

Suwanda, R., Z. Syahputra, and E.M. Zamzami. 2020. Analysis of Euclidean Distance and Manhattan Distance in the K-Means Algorithm for Variations Number of Centroid K. *Journal of Physics: Conference Series* 1566, 4th International Conference on Computing and Applied Informatics 2019 (ICCAI 2019): 26–27. November 2019, Medan, Indonesia.

Swales, D., M. Alexander, and M. Hughes. 2016. Examining moisture pathways and extreme precipitation in the U.S. Intermountain West using self-organizing maps. *Geophysical Research Letters* 43: 1727–1735. doi:10.1002/2015GL067478.

Tarek, M., F.P. Brissette, and R. Arsenault. 2020. Evaluation of the ERA5 reanalysis as a potential reference dataset for hydrological modelling over North America. *Hydrology and Earth System Sciences* 24(5): 2527–2544.

Zeng, X., P. Broxton, and N. Dawson. 2018. Snowpack Change From 1982 to 2016 Over Conterminous United States. *Geophysical Research Letters* 4: 12940–12947. https://doi.org/10.1029/2018GL079621

Appendix A

Historical Snowfall Dates

Table A-1.—Top eight observed historical snowfall events in each basin, along with the weather type associated with that event. Events are ranked from oldest to newest.

Methow basin		Snake River basin		Sun River basin		Truckee-Carson basins		Upper Klamath Lake basin		Upper San Juan basin	
Date	Weather Type	Date	Weather Type	Date	Weather Type	Date	Weather Type	Date	Weather Type	Date	Weather Type
01/18/1986	1	02/17/1986	1	02/16/1986	2	01/4/1982	1	12/8/1992	1	11/30/1982	0
12/9/1987	0	02/19/1986	0	11/24/1990	1	02/16/1986	0	01/23/1996	2	02/4/1989	0
10/31/1994	0	03/4/1991	1	04/11/1991	2	12/21/1996	0	01/22/1999	2	02/19/1993	1
11/7/1995	0	11/18/1996	0	10/31/1994	0	12/2/2001	1	01/10/2000	2	03/28/1998	0
12/29/1996	0	01/11/1998	2	12/29/1996	0	12/16/2002	1	12/8/2004	0	01/11/2005	0
01/30/1997	1	01/19/2012	0	01/25/2002	1	01/4/2008	1	12/30/2005	0	12/1/2007	1
11/18/2003	1	11/25/2014	1	04/28/2009	0	01/10/2017	1	12/28/2010	1	12/7/2007	0
11/25/2014	1	01/10/2017	1	02/8/2018	0	02/20/2017	1	01/18/2012	1	01/5/2008	1

Appendix B

Anomalous Weather Conditions

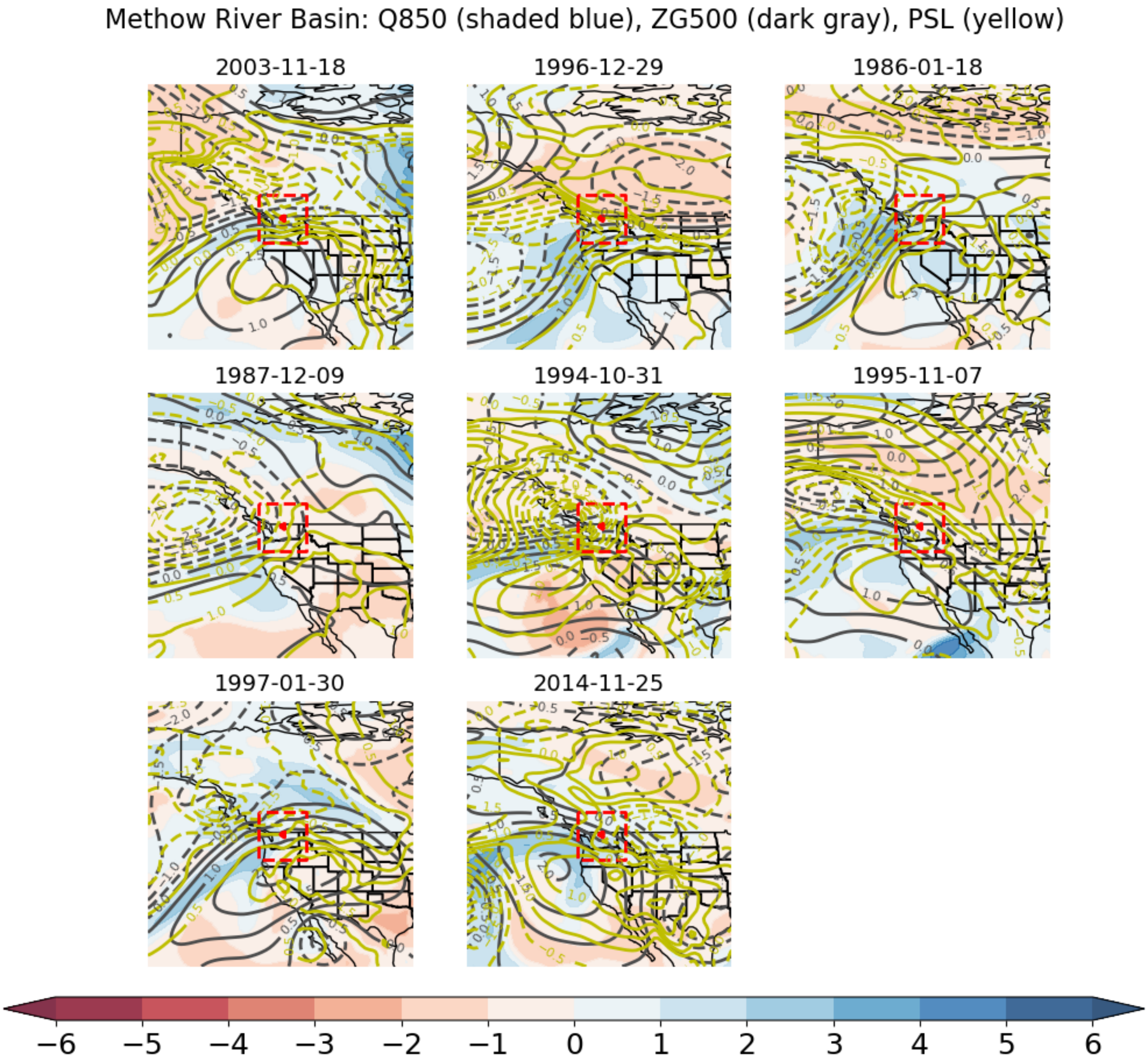

Figure B-1.—Anomalous weather conditions for each of the top eight daily snowfall events for the Methow River basin ranked from greatest to lowest snowfall totals. Shading represents anomalies of 850 hPa specific humidity, dark grey lines represent anomalous 500 hPa geopotential height, and yellow lines represent anomalous sea level pressure.

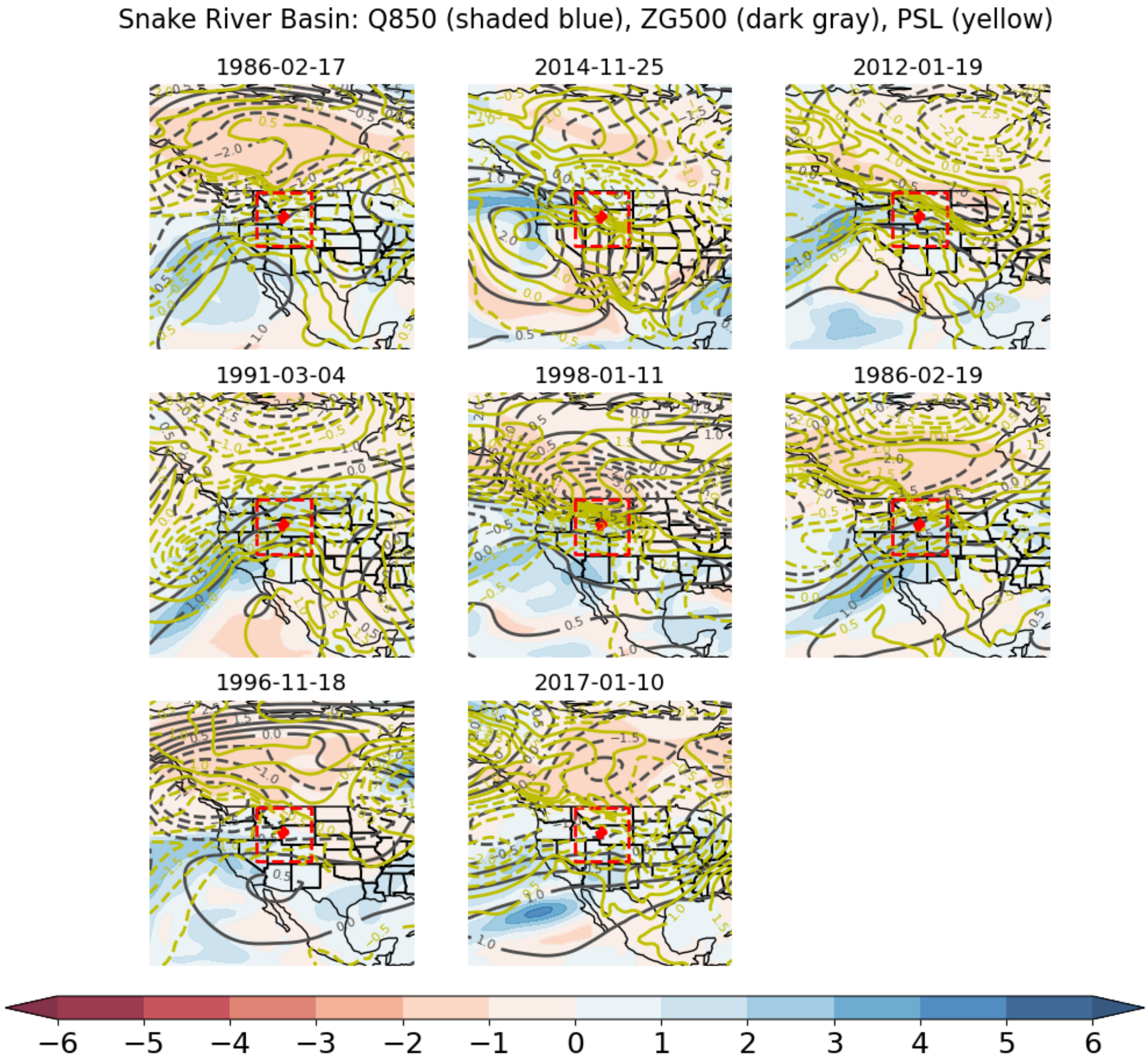

Figure A-B.—Same as figure B-1 except for the Snake River basin.

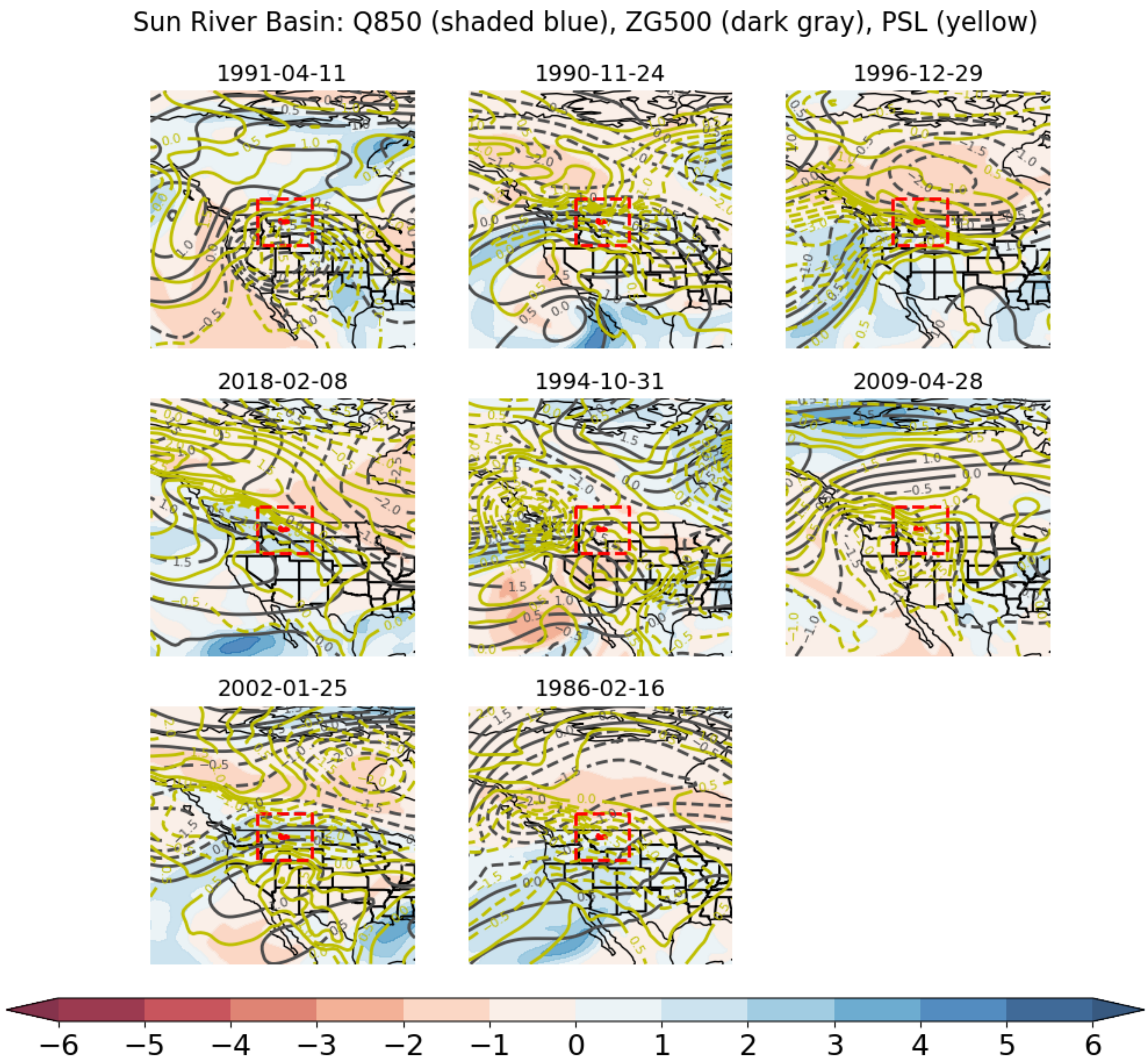

Figure B-3.—Same as figure B-1 except for the Sun River basin.

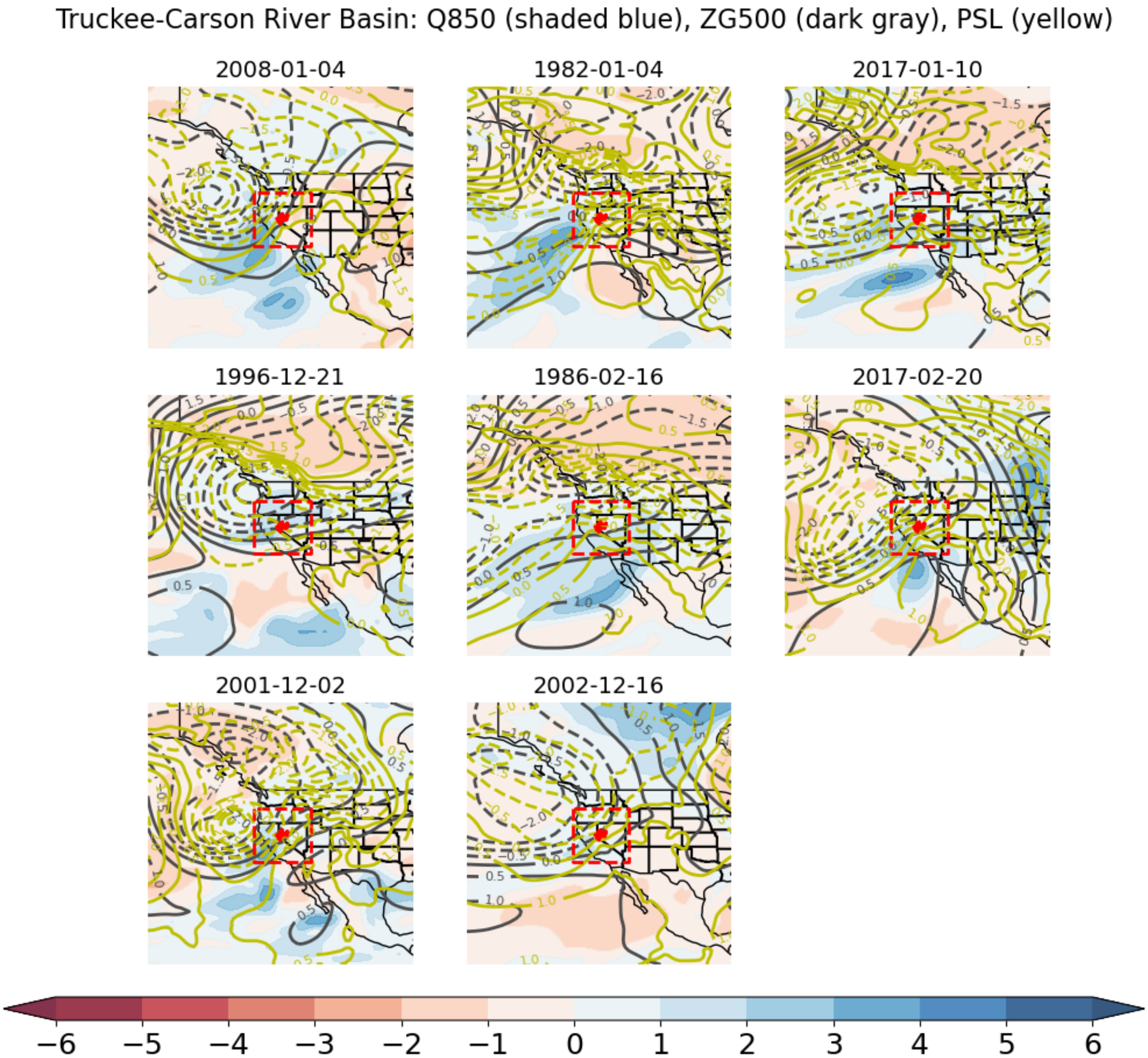

Figure B-4.—Same as figure B-1 except for the Truckee-Carson River basins.

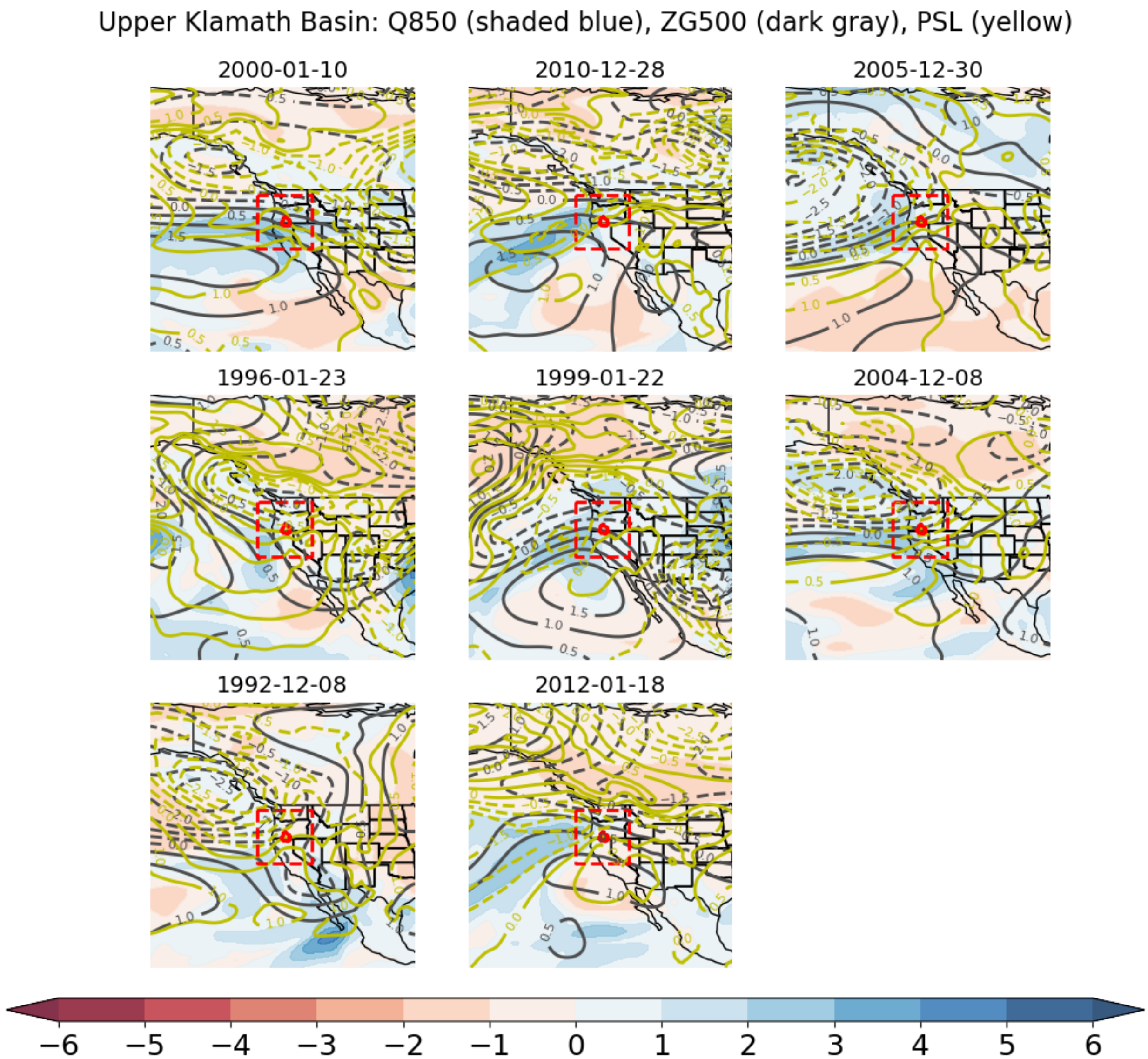

Figure B-5.—Same as figure B-1 except for the Upper Klamath basin.

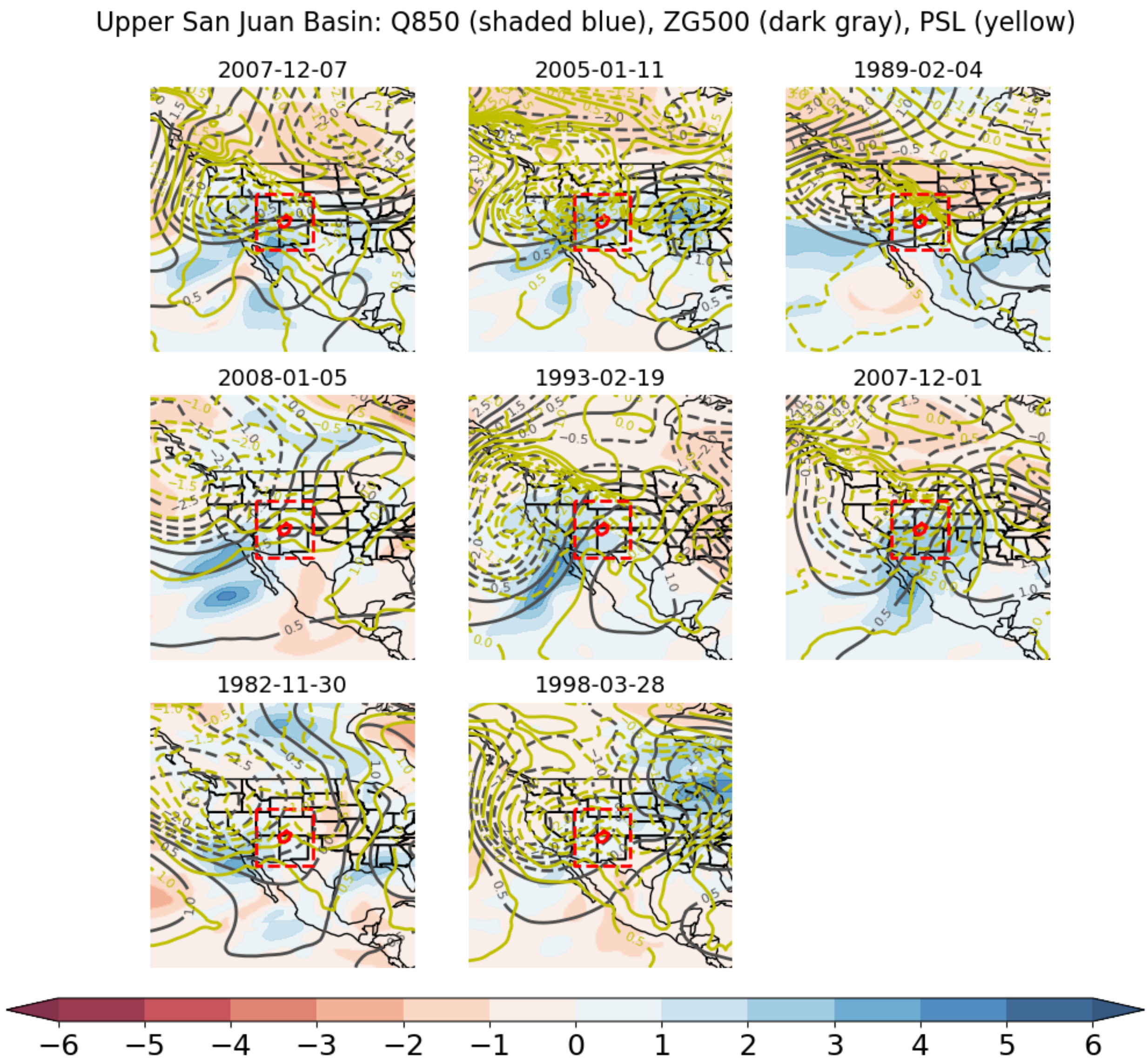

Figure B-6.—Same as figure B-1 except for the Upper San Juan basin.